UNIVERSITY OF THE WITWATERSRAND, JOHANNESBURG

EFFECTS OF NIOBIUM (Nb) ON MECHANICAL PROPERTIES OF LASER COATED NITINOL (NiTi) USED FOR SURFACE MODIFICATION OF Ti6Al4V ALLOY

MSc (50/50) DISSERTATION

Prepared by

Besabakhe Samuel Skhosane, Student No: 1510717

Submitted to

School of Chemical and Metallurgical Engineering, Faculty of Engineering and the Built Environment, University of the Witwatersrand, in the fulfilment of the requirement for the degree of Master of Science in Engineering

Supervisor(s): Prof Nthabiseng Maledi and Dr Monnamme Tlotleng

October 2021

Declaration

I hereby declare that the work submitted for my Master of Science in Welding Engineering at the University of the Witwatersrand is my own original work, and I further declare that all sources cited or quoted in this work are acknowledge by means of a comprehensive referencing.

Samuel Skhosane

Signature: ___________ Year _________2021____________.

Abstract

In the present study, mechanically pre-alloyed powders consisting of niobium, titanium and nickel were deposited onto Ti6Al4V substrate to form a coating with the aim of improving surface wear resistance. Laser cladding was used to melt the injected powder to form a coating on the surface of the substrate. Fabricated samples were produced from the powder mixture of $Ti_{55}Ni_{45}$, $Ti_{53.75}Ni_{43.75}Nb_{2.5}$, $Ti_{52.5}Ni_{42.5}Nb_5$ and $Ti_{51.25}Ni_{41.25}Nb_{7.5}$ using different laser power (600W and 1000W) and laser-scanning speed (0.5-1m/min) at fixed powder deposition rate of 2rev/min. The fabricated samples were characterised using optical microscopy (OM), scanning electron microscopy (SEM) with energy dispersive spectroscopy (EDS), differential scanning calorimeter (DSC), X-ray diffraction (XRD), micro hardness tester and wear tester. The produced coatings were well bonded and consisted of globular and dendritic structure with intermetallic phases such as NiTi and $NiTi_2$. Hardness decreased with an increase in niobium content while wear resistance enhanced, with no cracking on the coating surface as niobium content increased

Acknowledgments

I would like to take this opportunity to thank my supervisors, Prof Nthabiseng Maledi from the School of Chemical and Metallurgical Engineering at the University of the Witwatersrand and Dr Monnamme Tlotleng from Council for Scientific and Industrial Research (CSIR), for their leadership, their kindness and mostly for their motivations throughout my studies.

I also like to pass my thanks to all of my colleagues at CSIR -Manufacturing - National Laser centre (NLC), Prof Sisa Pityana, Dr Corney van royen, Mrs Marita Theron, Mr Khoro Malabi, Dr Ipfi Mathoho, Mr Phushetso Ramasobane and Mr Oscar Sono for their support and kindness and sharing their expertise with me concerning equipment operations and laboratory work.

My deepest appreciation to my wife, Mrs Zelda Skhosane for her support, understanding and her love during my studies. Studying, working and being a husband at the same time was not an easy task, but I`m so thankful that during this difficult time of Covid-19 I was blessed with a daughter (Ntando) and have manage to pull through with my MSc.

I would also like to thank my manager Dr Lerato Tshabala and the CSIR for giving me the opportunity and financially supporting for my studies.

Table of Contents

Declaration ii
Abstract iii
Acknowledgments iv
Table of Contents v
List of Figures viii
List of Tables x
List of Abbreviation xi
Chapter 1 Introduction 1
1.1. Background 1
1.2. Gaps and significance of this research 2
1.3. Problem statement 2
1.4. Research aim and objectives 2
1.5. Hypothesis 3
1.6. Delineations and limitations 3
1.7. Structure of dissertation 3
Chapter 2 Literature review 5
2.1. Metallurgy of titanium and its alloys 5
2.1.1. Alloying of pure titanium 5
2.1.2. Ni-Ti alloy 6
2.1.3. Mechanical properties and application of pure titanium (Grade 1) 8
2.1.4. Production of NiTi 9
2.1.5. Effect of niobium addition on TiNi-Nb alloy 10
2.1.6. XRD analyses of NiTi phases 12
2.1.7. Effect of Nb addition on Ti-Ni alloy and wear properties 12
2.1.8. Transition temperature of Ti-Ni alloy 13
2.2. Wear failure 14
2.2.1. Abrasive wear 14
2.2.2. Adhesive wear 15
2.3. Process techniques used for surface modification 15
2.3.1. Laser cladding 16
2.3.2. Laser cladding parameters 17
2.4. Summary of chapter 2 19

Chapter 3 Research methodology 20
3.1. Nominal composition of powders used 20
3.2. Blending and characterization of powders 20
3.3. Laser cladding process 21
3.4. Process parameter optimisation 23
3.4.1. Powder flow rate development 23
3.4.2. Laser parameter development 23
3.4.2.1. Single clad parameter optimisation process 23
3.4.2.2. Sample production 24
3.5. Material characterisation 24
3.5.1. Optical and scanning electron microscope 25
3.5.2. X-ray diffraction 25
3.5.3. Differential scanning calorimeter (DSC) 25
3.6. Mechanical testing 26
3.6.1. Wear testing 26
3.6.2. Hardness testing 26
3.7. Summary of Chapter 3 27
Chapter 4 Results and Discussion 28
4.1. Single clads 28
4.2. Multiple clads optical analysis 30
4.3. Optical microscope results of $Ti_{50-x/2}$ $Ni_{50-x/2}Nb_x$ 32
4.3.1. Optical micrographs of Ti50-x/2 Ni50-x/2Nbx produced at 600W laser power and 0.5m/min laser scanning speed 32
4.3.2. Optical micrographs of Ti50-x/2 Ni50-x/2Nbx produce at 1000W laser power and 0.5m/min laser scanning speed 33
4.4. SEM and Energy dispersive spectroscopy results of the coating 35
4.5. SEM microstructural analyses of $Ti_{50-x/2}$ $Ni_{50-x/2}Nb_x$ alloys 37
4.6. XRD results $Ti_{50-x/2}$ $Ni_{50-x/2}Nb_x$ alloys 39
4.7. Differential Scanning Calorimeter results 40
4.8. Hardness results 42
4.9. Wear test results 44
4.10. Summary of Chapter 4 46
Chapter 5 Conclusions 47
5.1. Summary of the findings 47

5.2. Recommendations 47
Chapter 6 References 49
Chapter 7 Appendix A: MRS Conference paper 20 54

List of Figures

Figure 2.1: Binary Ni-Ti phase diagram [24]. 7

Figure 2.2: Nitinol crystal structures during heating and cooling [2]. 8

Figure 2.3: Microstructure of laser printed Nitinol (Ti-Ni) [21]. 10

Figure 2.4: Pseudo-binary phase diagram of NiTi-Nb. [8] 11

Figure 2.5: XRD spectrum of NiTi, $NiTi_3Nb$, $NiTi_6Nb$ and $NiTi_9Nb$ alloy [8] 11

Figure 2.6: Wear resistance of NiTiNb clad and Ti6Al4V [5] 13

Figure 2.7: Abrasive wear mechanism [33] 15

Figure 2.8: Powder laser cladding process [11] 16

Figure 2.9: Schematic weld profile showing, HAZ, dilution and clad layer [38] 18

Figure 3.1: Powder morphology of $Ti_{51.25}Ni_{41.25}Nb_{7.5}$ 21

Figure 3.2: Laser cladding nozzle (3-way nozzle). 22

Figure 3.3: Single and multiple clads of Ti-Ni powder laser coated on Ti6Al4V 23

Figure 3.4: Vickers micro-hardness machine 27

Figure 4.1: Singe clads of Ti-Ni alloy, sample 1 produced at 600w with 0.5m/min, (2) at 600w with 1m/min, (3) at 1000w with 0.5m/min and (4) produced at 1000w with 1m/min. 28

Figure 4.2: Optical micrographs of Ti-Ni single clads produced at varying laser power and scanning speed (1) 600W and 0.5m/min, (2) 600W and 1m/min, (3) 1000W and 0.5m/min, (4) 1000W and 1m/min. 29

Figure 4.3: Multiple clads of Ti-Ni alloy with sample (a) produced at 600W at 0.5m/min, (b) 600W at 1m/min, (c) 1000W at 0.5m/min and (d) 1000W at 1m/min. 30

Figure 4.4: Optical micrographs of (a) $Ti_{55}Ni_{45}$, (b) $Ti_{53.75}Ni_{43.75}Nb_{2.5}$ (c) $Ti_{52.5}Ni_{42.5}Nb_5$ and (d) $Ti_{51.15}Ni_{41.15}Nb_{7.5}$ produce at 600W laser power and 0.5m/min laser scanning speed. 32

Figure 4.5: Optical micrographs of (a) $Ti_{55}Ni_{45}$, (b) $Ti_{53.75}Ni_{43.75}Nb_{2.5}$ (c) $Ti_{52.5}Ni_{42.5}Nb_5$ and (d) $Ti_{51.15}Ni_{41.15}Nb_{7.5}$ produce at 1000W and 0.5m/min 34

Figure 4.6: Optical micrographs of $Ti_{53.75}Ni_{43.75}Nb_{2.5}$ produced at laser power of 1000W and 0.5m/min scanning speed. 35

Figure 4.7: EDS analysis of $Ti_{55}Ni_{45}$ produced at 600W with 0.5m/min..........36

Figure 4.8: Overall EDS spectrum of $Ti_{51.15}Ni_{41.15}Nb_{7.5}$ produced at laser power of 600W and 0.5m/min laser scanning speed. 37

Figure 4.9: SEM micrographs of four typical $Ti_{50-x/2}$ $Ni_{50-x/2}Nb_x$ alloys: (a) $Ti_{55}Ni_{45}$, (b) $Ti_{53.75}Ni_{43.75}Nb_{2.5}$ (c) $Ti_{52.5}Ni_{42.5}Nb_5$ and (d) $Ti_{51.15}Ni_{41.15}Nb_{7.5}$ produced at 600W and 0.5m/min 38

Figure 4.10: XRD pattern of $Ti_{55}Ni_{45}$, $Ti_{53.75}Ni_{43.75}Nb_{2.5}$, $Ti_{52.5}Ni_{42.5}Nb_5$ and $Ti_{51.15}Ni_{41.15}Nb_{7.5}$ produced at laser power of 600W and scan speed of 0.5m/min 39

Figure 4.11: DSC curve of $Ti_{55}Ni_{45}$ sample produced at 600W laser power and 0.5m/min scanning speed 40

Figure 4.12: Heating and cooling DSC curve for $Ti_{51.25}Ni_{41.25}Nb_{7.5}$ alloy..........41

Figure 4.13: Microhardness profile of laser deposited $Ti_{50-x/2}$ $Ni_{50-x/2}Nb_x$ alloy coating 42

Figure 4.14: Hardness results of $Ti_{50-x/2}$ $Ni_{50-x/2}Nb_x$ alloy samples produced at 1000W laser power and 0.5m/min laser scanning speed. 43

Figure 4.15: Wear results of laser deposited $Ti_{50-x/2}$ $Ni_{50-x/2}Nb_x$ alloy coating..........44

Figure 4.16 SEM images of worn $Ti_{50-x/2}$ $Ni_{50-x/2}Nb_x$ alloys: (a) $Ti_{55}Ni_{45}$, (b) $Ti_{53.75}Ni_{43.75}Nb_{2.5}$ (c) $Ti_{52.5}Ni_{42.5}Nb_5$ and (d) $Ti_{51.15}Ni_{41.15}Nb_{7.5}$ produced at 600W and 0.5m/min 45

List of Tables

Table 2.1 Physical properties of pure titanium (grade 1) [13]. 5

Table 2.2 : Mechanical properties of grade 1 titanium [16]. 8

Table 2.3 : Reference peak positions for three phases of NiTi revised by Riva et al [28] , Chan et al [29] and Iijima et al [30] 12

Table 2.4: Comparison between laser cladding and TIG or MIG process [11].......................17

Table 3.1 : Chemical compositions of the powders in weight percentage..............................20

Table 3.2: Laser process parameters optimisation for single clad and double clads using Ti-Ni alloy...24

Table 3.3: Laser parameters for multiple clads of $Ti_{55}Ni_{45}$, $Ti_{53.75}Ni_{43.75}Nb_{2.5}$, $Ti_{52.5}Ni_{42.5}Nb_{5}$ and $Ti_{51.15}Ni_{41.15}Nb_{7.5}$ alloys. 24

Table 4.1: Dilution for the multiple clads of Ti-Ni alloy with sample (a) produced at 600W at 0.5m/min, (b) 600W at 1m/min, (c) 1000W at 0.5m/min and (d) 1000W at 1m/min 31

List of Abbreviation

OM	Optical microscope
SEM	Scanning Electron Microscope
EDS	Energy Dispersive Spectroscopy
DSC	Differential Scanning Calorimeter
Ti	Titanium
Nb	Niobium
Ni	Nickel
NiTi	Nitinol
SME	Shape Memory Effects
HAZ	Heat Affected Zone
m/min	meter per minute
rev/min	revolution per minute
L/min	Litre per minute
M_s	Martensite start
M_f	Martensite finish
A_s	Austenitic start
A_f	Austenitic finish
IPG	IRE-Polus Group
LASER	Light Amplification by Stimulated Emission
DMD	Direct Metal Deposition
W	Watt

Nd	Neodymium
CO_2	Carbon dioxide
COF	Coefficient of friction
CSIR	Council for Scientific and Industrial Research
NLC	National Laser Centre
ICDD	International Centre for Diffraction Data
XRD	X-ray diffraction
MRS	Material Research Society
FCC	Face Centred Cubic
BCC	Body-Centred Cubic

Chapter 1 Introduction

1.1. Background

Nitinol (NiTi) is a titanium alloy produced by alloying pure titanium with pure nickel at approximately equal atomic percent. This combination has brought special properties such as good superelasticity, shape memory effect, low stiffness, and good corrosion resistance [1, 2]. Scientist Buehler W.J. discovered shape memory effect of NiTi in 1959 when heating the folded strip of nickel and titanium returned to its original shape [3]. Nitinol alloy is used in the manufacturing of aircraft components, thermo-power actuators, and thermomechanical connectors. The alloy is also used in the manufacturing constrictive stents within the medical filed [4].

Across the world, the focus is on finding a solution for improving wear properties of Ti6Al4V material. Several coatings such as titanium nitride, electro plating of nickel, chromium, cobalt, and NiTi) were previously exploited for surface modification of Ti6Al4V with the aim of improving its wear resistance [1, 5]. Titanium nitride (TiN) coating, which is mostly used in the coating of tool steel was exploited using plasma nitriding and high velocity oxy-fuel (HVOF). However, these processes failed because of the high heat inputs induced by the processes, which increases dilution and affect mechanical properties [1, 5].

A promising solution for surface modification of Ti6Al4V that has not been fully exploited is the deposition of nitinol coating onto Ti6Al4V substrate [1, 5]. Metallurgically, NiTi slloy is the best choice for coating Ti6Al4V since it contains about 50% titanium, which makes it more compatible and has better wear properties than Ti6Al4V [1, 5]. NiTi alloy has better sliding wear resistance than steel, nickel base and cobalt base material [6]. However, NiTi alloy has poor machinability [7] due to its high hardness.

The desire to enhance mechanical properties of NiTi alloy, especially its surface wear resistance and machinability has brought the idea of adding a third element such as niobium [5, 8, 9]. Niobium (Nb) has a body-centred-cubic (BCC) crystal structure. Nb is light grey in colour and has a melting point of 2477°C. It is mainly used as a micro-alloying element in steels to prevent recrystallization by pinning the grain boundaries, which also suppresses the phase transformation from austenite to ferrite. It is also used as a key alloying element to strengthen nickel-base material [10]. Addition of Nb in Ni-Ti alloy forms lubricating composite Nb_2O_5 which improves the surface wear resistance [9] .

1.2. Gaps and significance of this research

Over the past years, most researchers have studied the effect of niobium content in the microstructural, mechanical properties and thermal characteristics of NiTiNb using different processes. Tian et al. [5], used a preplacement powder laser cladding method to deposit TiNiNb clad onto Ti6Al4V. Their method was successful however, laser cladding by powder preplacement technique is limited to processing of flat surfaces. Li et al. [9] implanted niobium ions using metal vapour vacuum arc plasma source (MEVVA), achieving 46%-62% reduction in wear width. However, MEVVA process is known to induce high heat input than laser cladding process, which produces low heat input, low dilution and low heat affected zone (HAZ) [11]. There is limited work reported on laser cladding of a pre-alloyed TiNiNb using direct metal deposition (DMD) method. This work, focused on studying the effect of niobium on mechanical properties and processability of TiNiNb as produced by laser cladding a pre-alloyed powder of TiNiNb alloy using DMD laser cladding technique.

1.3. Problem statement

Titanium alloy (Ti6Al4V) has excellent corrosion resistance and good creep resistance. However, the use of this titanium alloy is limited due to its poor wear resistance properties. These limitations can be overcome by performing surface modification or coating with NiTi alloy since it has superelastic behaviour [6]. NiTi coating has good wear resistance properties [1, 6] and can easily bond to Ti6Al4V surface. However, NiTi coating is very brittle [7]; thus, there is a need to enhance its mechanical properties before it can be considered as a surface coating for Ti6Al4V alloy.

1.4. Research aim and objectives

The aim of this study is to enhance mechanical properties of nitinol coating by adding niobium using laser deposition method to improve wear resistance of Ti6Al4V substrate.

This research focused on the following key objectives:

- Investigating laser process parameters for the deposition of pre-alloyed powders.

- Study the effect of niobium addition on the microstructure and transition temperature of nitinol.
- Evaluate the effects of niobium (Nb) on mechanical properties (hardness and wear resistance) of laser coated nitinol (NiTi) used for surface modification of Ti6Al4V alloy

1.5. Hypothesis

It was hypothesised that mechanical properties of NiTi alloy may be enhanced by adding niobium. This can be achieved by depositing mechanically mixed pure powders of titanium, nickel and niobium on Ti6Al4V base using laser cladding process in DMD technique rather using preplacement powder laser cladding method or metal vapour vacuum arc plasma source (MEVVA).

1.6. Delineations and limitations

In this study, mechanically pre-alloyed powders of niobium, nickel and titanium was laser deposited on Ti6Al4V substrate using laser equipment available at the National Laser Centre (NLC), CSIR. Nitinol clads were produced by varying the niobium content added to Ti/Ni ratio of 1.22 wt.% of each alloy fabricated by varying laser power at fixed scanning speed and fixed powder flow rate.

1.7. Structure of dissertation

This dissertation presents the effect of Nb on microstructure and mechanical properties of nitinol alloy. The following summarise the structure of the dissertation:

Chapter 1 presents the introduction, aim, objectives problem statement and the hypothesis of the study.

Chapter 2 focused on literature review, addressing important findings reported by previous authors on Ti-Ni alloy. It is shown that the shape memory effect of Ti-Ni alloy is present when composition of titanium and nickel are in equal ratio. Alloying of nitinol with third element such as niobium enhances mechanical properties.

Chapter 3 presents detailed experimental procedure used for the studying effect of process parameters and varying Nb composition on mechanical properties of nitinol.

Chapter 4 presents the results and discussion of the investigation

Chapter 5 presents conclusions and recommendations from the study.

The list of references are included in Chapter 6, with a conference paper appended in Chapter 7.

Chapter 2 Literature review

This chapter focused on reviewing previous research studies relating to titanium and titanium alloys processed by different techniques including laser cladding, and electric arc furnace etc. Most recent studies looked at surface modification of Ti6Al4V by depositing Ti-Ni or Ti-Ni-Nb alloy using either electric furnace or laser as a heat source. Few studies looked at enhancing the wear resistance of Ti-Ni alloy by adding Nb using laser.

2.1. Metallurgy of titanium and its alloys

Titanium and titanium alloys have two allotropic phases which are the alpha (α) and beta (β) phase. The alpha phase of titanium has a hexagonal closed packed (HCP) crystal structure, and the β-phase has a body centred cubic (BCC) crystal structure. In pure titanium, the α-phase is stable below 882°C and the β-phase is stable above 882°C [12].

The properties of titanium and titanium alloy originate from the orientation of the crystal structure and the proportion of α and β phase within the material. Physical properties of commercially pure titanium (Grade 1) alloy are shown in Table 2.1.

Table 2.1 Physical properties of pure titanium (grade 1) [13].

Physical properties	Value
Melting temperature	1680°C
Boiling point	3287°C
Density of liquid	4.11 g/cm^3
Density of solid (near room temperature)	4.506 g/m^3
Thermal conductivity	16.3 Wm^{-1}.K^{-1}

2.1.1. Alloying of pure titanium

The main purpose of alloying pure titanium is to increase its strength, hardness, wear resistance and corrosion resistance so that it can perform better and expand their use in different industries. Alloying is one of metal strengthening techniques. The degree of solid solution strengthening depends on two factors: firstly, a larger difference in atomic size between the original atom and the added atom increase the strengthening effect, this is due to disruption caused on the crystal lattice, and secondly the amount of the alloying elements added [14].

Ti6Al4V alloy is a titanium alloy that has improved strength. It is formed by alloying pure titanium with 6wt. % aluminium and 4wt. % vanadium. Aluminium is an alpha phase stabiliser alpha phase beyond 882°C. Although Ti6Al4V has good strength and corrosion resistance at higher temperature [15], it has poor sliding wear properties [1, 16]. This can be modified by applying a wear resistance coating such as Ni-Ti alloy on its surface [1, 6].

Another element used in alloying pure titanium for production of nitinol is nickel. Nickel is naturally present in the Earth`s crust. Commercially pure nickel (99.5%) is white in colour, and it is known by its good corrosion resistance in water and in air [17]. Nickel has face-centred-cubic crystal structure and a melting point of 1453°C. It is one of the toughest materials used in both cryogenic and elevated temperatures [17]. Nickel can only be hardened and strengthened by cold working [18]. Mechanical properties of nickel are highly influenced by its purity. Commercially pure nickel contains impurities such as carbon, cobalt, iron, silicon, and sulphur, which affect its strength [18]. It is used in the manufacturing of aerospace components such as turbine blades and engine casings due to its good corrosion resistance and high temperature properties [19].

2.1.2. Ni-Ti alloy

Nitinol or NiTi alloy is one of the titanium alloys produced from pure nickel and pure titanium, where the two elements are present roughly in equal atomic percentages [20]. Nitinol has remarkable properties such as superelasticity, shape memory effect (SME), good corrosion resistance and low stiffness [1, 21, 22]. However, NiTi alloy has poor machinability [20, 7]. Its wear resistance depends on the ratio of Ti/Ni. The $Ti_{50}Ni_{50}$ wears faster than $Ti_{55}Ni_{45}$ [1], nonetheless, both have much better wear resistance than Ti_6Al_4V. Nitinol contains a very stable and self-healing layer (TiO_2) which makes it a better corrosion resistant alloy than stainless steel [23].

From the binary phase diagram shown in Figure 2.1, Ni-Ti alloys contains NiTi, $NiTi_2$ and Ni_3Ti intermetallic phases that form at different temperatures and compositions [24]. Near stoichiometric composition, TiNi intermetallic phase forms, whereas, at titanium rich region,

$NiTi_2$ intermetallic phase forms. The Ni_3Ti intermetallic forms in the nickel rich region [24]. The TiNi intermetallic phase has good ductility and toughness than $NiTi_2$ [1].

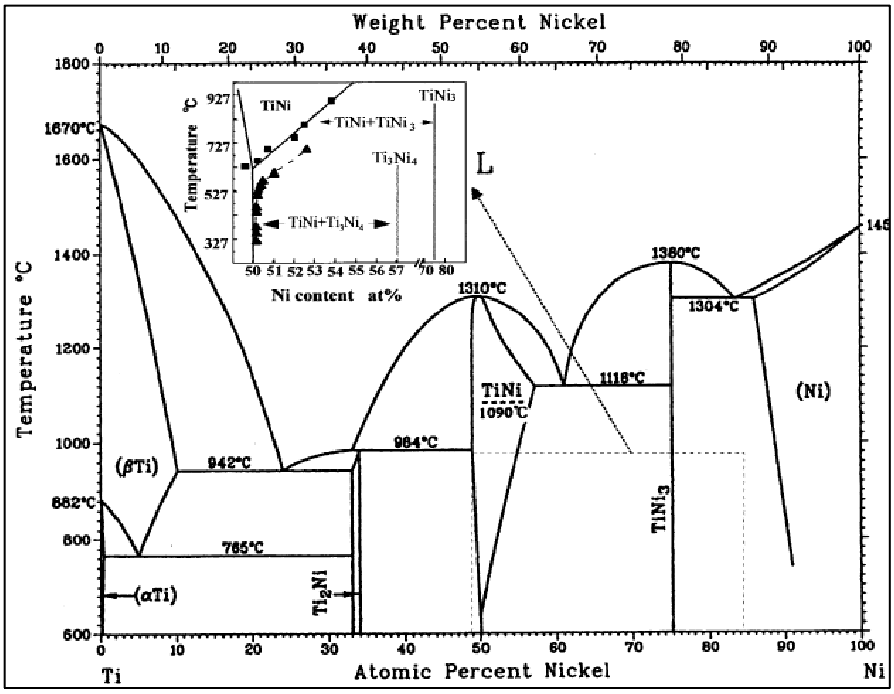

Figure 2.1: Binary Ni-Ti phase diagram [24].

Nitinol is comprised of the austenitic and martensitic phase. For the SME, NiTi transformation is between cubic crystal structures or austenite phase denoted as B2 phase and monoclinic or martensitic called B19 [2]. Martensitic crystal structure of nitinol has the unique ability to undergo limited deformation without breaking. It can also be reverted to austenite by heating as shown in Figure 2.2 regardless of whether the martensitic phase formed by deformation [2]. The martensitic phase can occur in one or two transformation steps, either by $B2 \rightarrow B19'$ or $B2 \rightarrow R \rightarrow B19$ [24]. The R-phase is distorted martensite that contains austenite phase. It is formed during austenitic cooling where one of the lattices elongates diagonally resulting in a reduced angle below 90 degrees [2]. The presence of rhombohedral or transformation of austenite to R-phase reduces the martensitic-austenitic thermal hysteresis, in turn reducing the superelasticity stored energy [25].

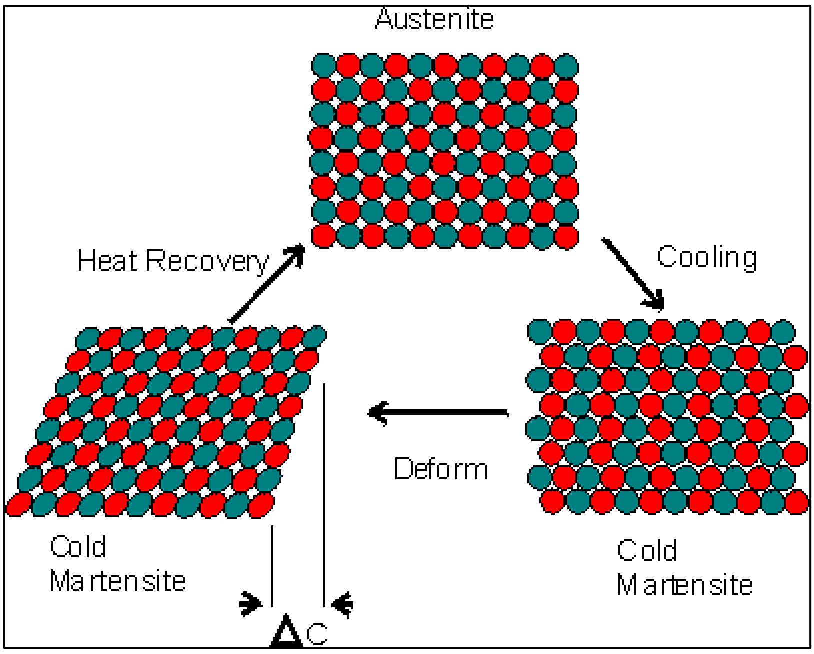

Figure 2.2: Nitinol crystal structures during heating and cooling [2].

Nitinol has found more application ranging from the aerospace to biomedical industry due to its excellent corrosion resistance [21]. Nitinol alloy has superplastic, SME properties and have better wear resistance than Ti6Al4V [1, 2].

2.1.3. Mechanical properties and application of pure titanium (Grade 1)

Mechanical properties of pure titanium are characterised by a combination of strength and ductility. Mechanical properties (tensile strength, yield strength, percent elongation and hardness) of Grade 1 titanium are summarised in Table 2.2

Table 2.2 : Mechanical properties of grade 1 titanium [16].

Property	Value
Tensile strength	240 MPa
Yield strength	170 MPa
Percent elongation	≥24%
Hardness	120HV

Mechanical properties of pure titanium are affected by the level of impurities such as oxygen, carbon, hydrogen, and iron. Grade 1 titanium is commonly used for floor support structures and tubes or pipe in the lavatory system [16].

2.1.4. Production of NiTi

There are several method that are used for processing nitinol, these include the use of laser additive manufacturing techniques (AM) such as selective laser melting (SLM), also known as laser powder bed fusion technology [2] and the use of direct metal deposition (DMD) [1], metal vapour vacuum arc plasma source also known as plasma spray [9] and electric arc-melting furnace process [8] . For surface coating, methods such as plasma nitriding, plasma spray, High Velocity Oxy-fuel (HVOF) and laser cladding are commonly used. Laser cladding is preferred amongst all these techniques since it produces less heat input without affecting the properties of the substrate [11].

Since Ti6Al4V alloys have poor wear resistance, most researchers worldwide are focusing on developing a wear resistance coating to improve the performance of Ti6Al4V alloys. Mokgalaka et al [1] studied nitinol coating, a mixture of titanium and nickel powders onto Ti6Al4V substrate. The powders were mixed using a ball mill and laser deposited onto the Ti6Al4V base plate to form a coating. The reported hardness of the Ti_{55}-Ni_{45} coating was 900 HV, higher than the hardness of the substrate which was 370 HV. The wear rate decreased from 14 mm^3/s for Ti6Al4V to 2.7mm^3/s for $Ti_{55}Ni_{45}$ coating. Abioye et al. [21] reported a microstructure of NiTi as shown in Figure 2.3 produced from laser cladded Ni-Ti powder. This microstructure has two distinct phases, a light grey dendritic structure marked “A” and a dark grey matrix marked “B”.

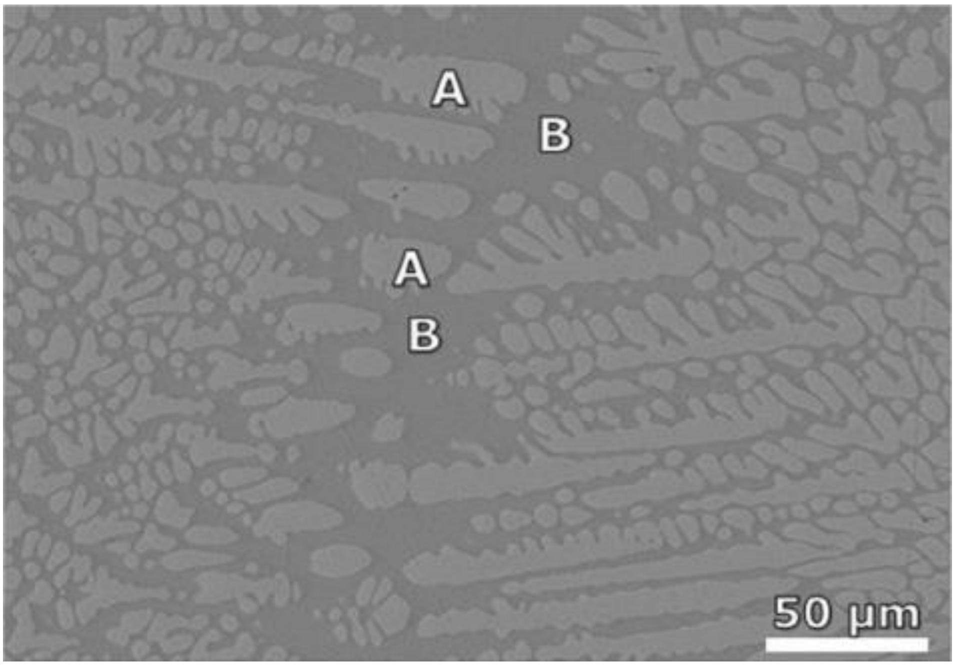

Figure 2.3: Microstructure of laser printed Nitinol (Ti-Ni) [21].

According to Abioye et al. [21], the phase marked “A” corresponded to NiTi intermetallic and the phase marked “B” correspond to $NiTi_2$.These phases were correlated to their chemical composition determined by energy dispersive spectroscopy (EDS). High hardness measured at the interface was related to high proportion of $NiTi_2$ phase observed at the interface.

2.1.5. Effect of niobium addition on TiNi-Nb alloy

Recent studies are now focusing on enhancing mechanical properties of nitinol by adding a third element such as Zr, Pd, V, Al or Nb to form a ternary system [26]. Shape memory characteristics and transformation are improved by adding Nb to form a ternary alloy. Ti-Ni-Nb alloys exhibits a wide transformation hysteresis and improves SME which is more beneficial in pipe couplings [8, 27].

Cronemberge et al. [8] has recently investigated the effect of Nb on microstructural and thermal characteristics of NiTi, ingot of pure nickel (99.9%Ni), pure titanium (99.3%Ti) and Nb (99.8%) were weighed and melted in electric arc furnace. Addition of Nb on a shape memory alloy (NiTi) formed a pseudo binary system as shown in Figure 2.4 (TiNi-Nb).

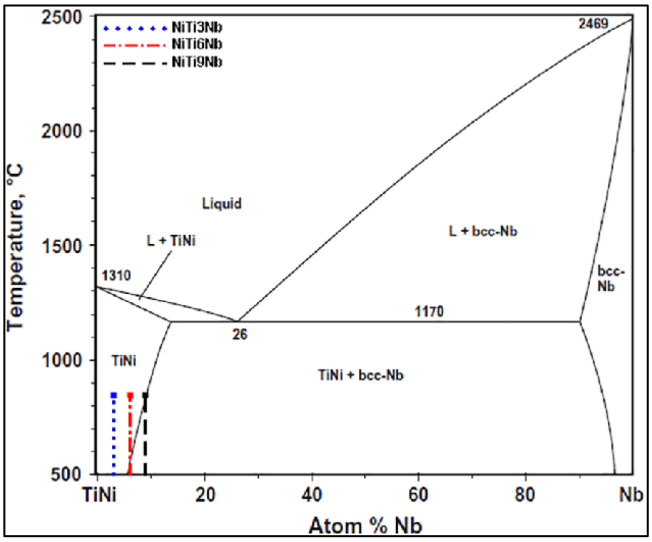

Figure 2.4: Pseudo-binary phase diagram of NiTi-Nb. [8]

An increase in Nb addition from 3 -9at. %, reduced both titanium and nickel composition which changed the Ti/Ni ratio. From the NiTi – Nb pseudo-binary phase diagram depicted in Figure 2.4, it is observed that an increase in niobium, shifts the reaction towards the eutectic reaction. Cronemberge et al [8] further analysed the samples using XRD to study the presence of intermetallic phases within these alloys (Figure 2.5).

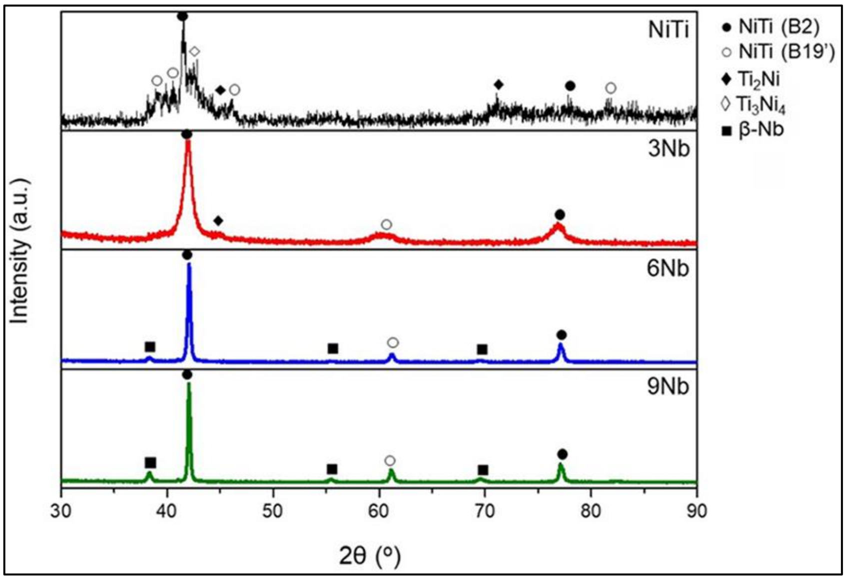

Figure 2.5: XRD spectrum of NiTi, $NiTi_3Nb$, $NiTi_6Nb$ and $NiTi_9Nb$ alloy [8]

The XRD results on NiTi alloy in Figure 2.5 show the existence of primary phase of NiTi (B2), secondary phase NiTi (B19), Ti_2Ni and Ti_3Ni_4 intermetallic [8]. Whereas NiTi alloy with 6 and 9 wt. % Nb does not have Ti_2Ni and Ti_3Ni_4 phase, instead, it has beta-niobium rich phase. The addition of Nb in Ti-Ni alloy suppressed the formation of $NiTi_2$ brittle phase [7], subsequently improving machinability.

2.1.6. XRD analyses of NiTi phases

The XRD peak positions of NiTi were analysed referring to the International Centre for Diffraction Data (ICDD) standards. Riva et al. [28], Chan et al. [29] and Iijima et al. [30] have reported XRD peak positions for NiTi phases using ICDD standard 18-0899 and ICDD standard that are shown in Table 2.3.

Table 2.3 : Reference peak positions for three phases of NiTi revised by Riva et al [28] , Chan et al [29] and Iijima et al [30] .

	Austenite (BCC) ICDD standard 18-0899	**Martensitic(monoclinic) ICDD standard 35-1281**	**R-phase(rhombohedral) River et al [28], Chan et al [29] and Iijima et al [30]**
2ϴ	**hkl plane**	**hkl plane**	hkl plane
39.22		020	
41.36		$1\bar{1}1$	
42.2			**112**
42.7			**300**
42.8	110		
43.92		002	
44.92		111	
61.58			**222**
61.98	200		
77.82			**412**
78.16	211		
78.16			**330**

2.1.7. Effect of Nb addition on Ti-Ni alloy and wear properties

In support on the development of an alloy that have good wear resistance, Tian et al. [5] conducted a study on surface modification of Ti6Al4V by laser cladding with a mixture of Ni-Ti-Nb powder. Their reported results revealed that surface modification of Ti6Al4V by laser cladding with Ni-Ti-Nb improved surface mechanical properties such as wear and hardness resistance, the reported hardness of the modified surface was twice that of the unmodified Ti6Al4V, with significant improvement in wear-resistance as shown in Figure 2.7.

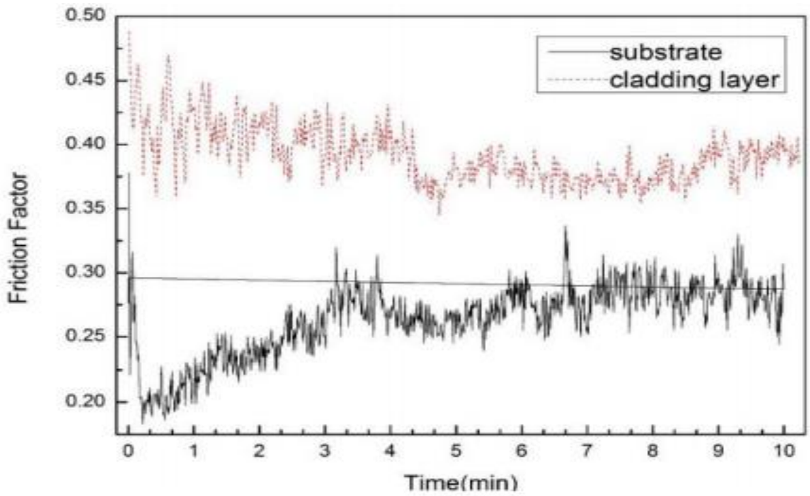

Figure 2.6: Wear resistance of NiTiNb clad and Ti6Al4V [5]

Li et al. [9], also investigated the effect of niobium on the wear properties of NiTi. Niobium ions were implanted in NiTi shape memory alloy polished surface using metal vapour vacuum arc plasma source (MEVVA 100). About 46%-62% reduction in wear width and about 29%-49% reduction in wear depth was reported [9]. Niobium had a significant influence on the increase in wear resistance; when implanting Nb on titanium surface, lubricating composite of Nb_2O_5 formed, thus improving the surface wear resistance [9].

2.1.8. Transition temperature of Ti-Ni alloy

Implantations of Nb in NiTi alloy comes with several characteristics. For example, addition of niobium alters the martensitic start and martensitic finish of nitinol, whereas SME relies on both martensitic and austenite. Cronemberger et al. [8], Chan et al. [29] and Alpati et al. [31] reported the effect of niobium addition on thermal hysteresis of nitinol. Cronemberger et al. [8] reported austenitic and martensitic transition temperature of Ti-Ni alloy with the value of A_s and A_f at 20°C and 39°C, respectively. M_s was recorded at 5°C and M_f at -5°C. The addition of 6 wt. %Nb slightly decreased the thermal hysteresis to A_s temperature of 17°C, and A_f temperature of 37°C, while $M_{s,}$ was recorded at -16°C and A_f at - 33°C. The thermal hysteresis decreased even further when the concentration of Nb was increased.

Chan et al. [29] also measured austenitic and martensitic transition of the as-received Ti-Ni alloy. From the study, the temperatures of $A_{s.}$ and $A_{f..}$ were recorded at 60.5°C and 95.6°C respectively, while martensitic transformation was found at M_s temperature of 66.2°C and M_f temperature of 24.8°C. There was a difference in the thermal hysteresis reported by Chan et al. [29] and Cronrmberger et al. [8]. The differences were due to variations in the process used or the ratio of Ti/Ni used.

Beritilsson et al. [24] reported transition temperatures of Ti-Ni alloy measured using DSC. The first endothermic peak was observed at temperature between 770 - 850°C during heating of the sample. This peak was associated with allotropic transition temperature of α-Ti to β-Ti, in pure titanium. This transition is known to occur at 882°C [12]. The second exothermic peak was observed in the temperature ranging from 946 -953°C. The peak was associated with the formation of the liquid when β-Ti and NiTi melted. The third peak was associated with the transformation from the solid to the liquid phase ($NiTi + Ni_3Ti = L$) at 1118°C.

2.2. Wear failure

Wear failure is defined as surface damage on a material or a loss of material particles on the surface. There are several wear failures within industries, such as sliding wear, abrasive wear, corrosion wear, erosion wear and fatigue wear. The basic wear mechanism in titanium alloys begin with abrasion, followed by adhesion wear [32].

2.2.1. Abrasive wear

Abrasive wear occurs when harder material is rubbing against softer material [33], as seen in Figure 2.6. The present of debris or harder particle between the components sliding on each other or the rough surface of the harder component may cut the softer surface or penetrate into the softer surface leading to the formation of cracks as can be seen in Figure 2.6 (a) and (b). The abrasive wear mechanism in Figure 2.6 (c) and (d) represent sharp hard particle cutting the softer material. Since Ti6Al4V alloy has a lower hardness than chromium, nickel, and cobalt, if titanium is paired with one of these materials under mechanical action, cutting wear mechanism or abrasion might occur on its surface.

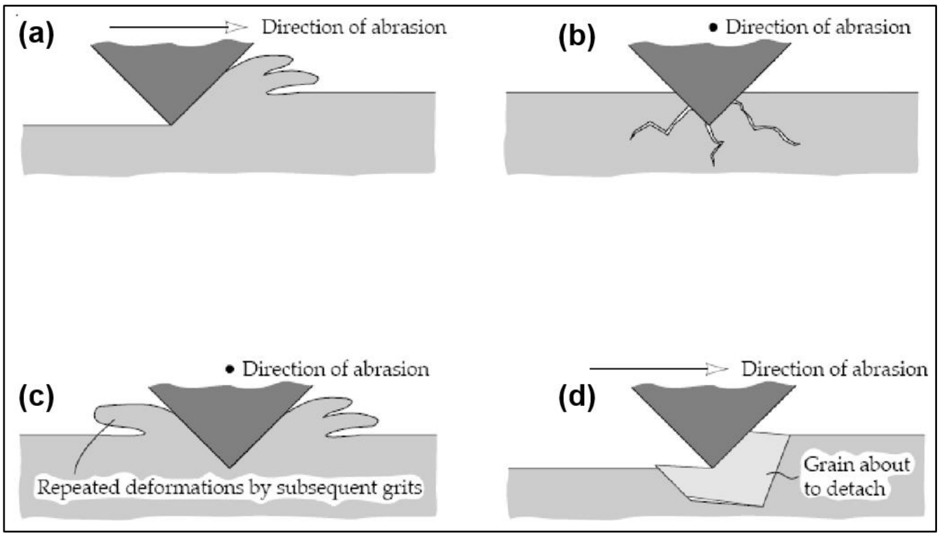

Figure 2.7: Abrasive wear mechanism [33]

Surface modification may extend the wear resistance [34]. Wang et al. [35] reported that surface coating titanium alloy with a hard coating of Ti_2Ni_3Si alloy improved abrasive wear and sliding wear.

2.2.2. Adhesive wear

Adhesive wear is a failure mechanism where two materials rub against each other, causing removal of softer material particles to adhere onto harder material [32]. Titanium alloy (Ti6Al4V) suffers from both abrasion and adhesive wear severely [32], due to its lower hardness. However, when it is coated with nitinol, adhesive and abrasive wear resistance of Ti6Al4V improves [1].

2.3. Process techniques used for surface modification

There are several surface modification techniques within the engineering industry that can be used for surface modification. Laser cladding, nitriding and thermal spraying are amongst surface coating techniques used in surface engineering. Recent focus is on using laser cladding since it has better advantages compared to other conventional coating process which includes less dilution and minimum HAZ [1, 11]

2.3.1. Laser cladding

Laser cladding process also called laser surface treatment is a reliable technique used to repair worn components in the engineering industry. It is also used to hard-face components with the aim of improving the wear resistance properties or impact properties of the components. Laser cladding technique uses either powder or wire as a filler material. For good bonding, the filler material must have the same chemical composition as the base or must be compatible to the base material. Laser cladding has special characteristics and several advantages over other surface modification techniques such as thermal plasma spray and submerged arc cladding [11].

Good metallurgical bonding between the surface coating and the parent material with minimum dilution is achieved with laser cladding process as compared to thermal plasma spraying or submerged arc cladding [1]. Laser cladding process produces low heat input, low heat-input produces less distortion, less dilution and minimum heat affected zone [1, 11]. Figure 2.8 shows a schematic laser cladding technique where powder is used as a filler material. Powder laser cladding process also knowns as DMD process involves laser melting the powder by moving the laser over the stream of blown powder to produce a melt pool on the surface of the substrate.

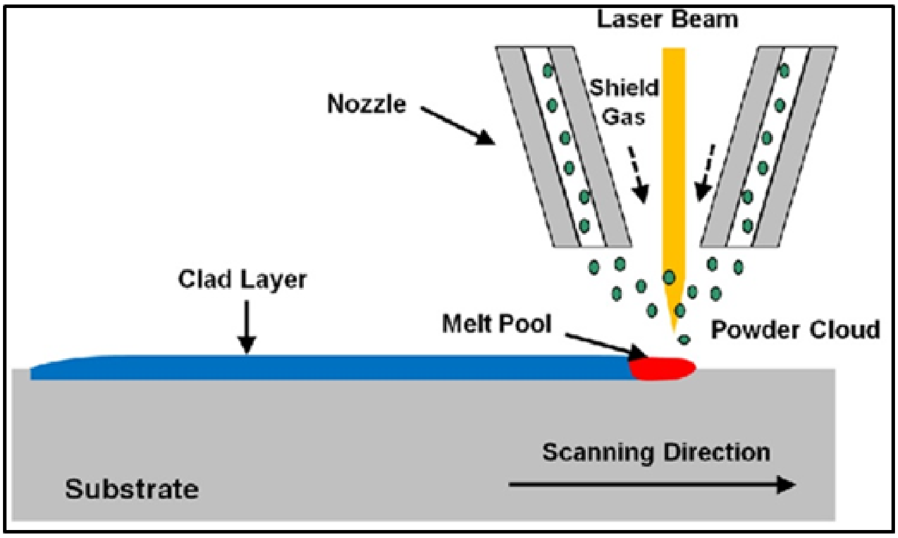

Figure 2.8: Powder laser cladding process [11]

The motion of the laser nozzle is guided by a CAD system from the robot arm which interpolates solid objects into a set of tracks, thus producing the desired part at the end of the trajectory. A laser beam is used as a heat source to melt the filler (powder or wire) and create weld pool that bond to a surface of the base material, which produces high quality, excellent metallurgical bond, and relatively thick coating on damaged or worn components [11].

Laser cladding setup involves defocusing the laser beam. Defocusing the laser beam changes the laser intensity from keyhole mode to conduction mode. It is more beneficial to use a lager laser beam diameter for cladding purposes since more powder can be entrapped and melted and this is also productive as relatively thicker and wider clads of high quality, excellent metallurgical bond can be achieved [11]. Table 2.4 compares TIG or MIG with laser cladding. More than 10% dilution is realized with TIG process, whereas laser can be controlled to yield less than 5% dilution.

Table 2.4: Comparison between laser cladding and TIG or MIG process [11]

Process out-put	**TIG or MIG welding**	**Laser Cladding**
Dilution rate	Approx. 10-40%	<5%
Use of filler material	More and non-uniform	Less and uniform deposition
Hardness value	Relatively low	Relatively high
Heat affected zone	Large and wide	Low and narrow
Surface finishing	Rough	Smooth
Pre and post treatment	More	Few
Dendrite structure and grains	Coarse	Fine
Automation	Difficult, low production rate and costly	Easy, high production rate and cost effective

2.3.2. Laser cladding parameters

There are several important parameters that determine the output quality of laser cladded component. These include laser scanning speed, laser power, laser beam diameter, powder feed rate and shielding gas [11]. However, laser power and laser scanning speed have considerable influence of the microstructure and the bonding of the clad [36, 37]. The ratio of laser power (P) and scanning speed (V) in Equation 1 describes the linear energy density (LED) which is the key factor on heat input. Heat input has serious effect on the toughness of the base material in the heat-affected zone (HAZ), dilution and deformation of base material. High heat input produces high dilution, and high heat input may cause deformation especially on thin bases. The ratio of laser power and scanning speed influence the solidification rate of the clad, higher laser scanning speed promotes fast cooling which results in refinement of microstructure, which in turn result in increased hardness [37]. Linear energy Equation 1 helps in determining laser energy density and controlling the heat input.

$$\text{Linear energy desity(LED)} = \frac{\text{Laser Power(P)}}{\text{Laser scanning speed(V)}*\text{Beam diameter(D)}} \qquad \text{Equation (1) [37]}$$

.

Generally, an increase in laser power increases the temperature significantly. However, increasing laser scanning speed slightly decreases the temperature [36]. Decreasing laser beam diameter increases laser intensity. Good laser parameters yield good clad quality. Quality coating is characterised by free defects, good metallurgical bond, good fusion, and minimum dilution. Figure 2.9 shows the schematic laser clad profile.

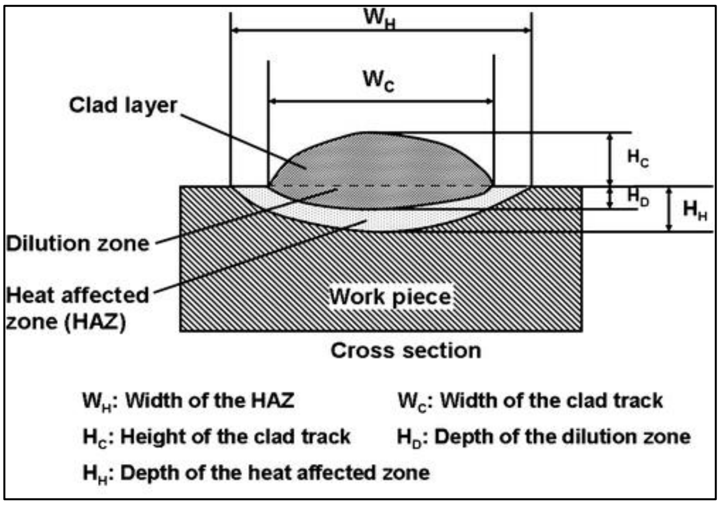

Figure 2.9: Schematic weld profile showing, HAZ, dilution and clad layer [38]

High dilution results from higher heat input, which is due to combination of higher laser power and lower scanning speed. Dilution is the mixture of the metal surface and the deposited clad and be measured using Equation 2.

$$\text{Percent dilution} = \frac{HD}{HC+HD)} * 100 \qquad \text{Equation (2)}$$

Where HD is the depth of dilution and HC measures thickness of the clad.

2.4. Summary of chapter 2

This chapter provided the literature about the metallurgy and characteristics of nitinol, the different processing route for producing nitinol, and the effects of niobium addition on mechanical properties and microstructure of nitinol. The effect of niobium addition of the transition and hysteresis temperatures for martensitic and austenitic start and finish temperatures were also evaluated. The benefits of using nitinol as coating on Ti6Al4V was highlighted. From this chapter, it was concluded that nitinol needs to be enhanced to improve its wear resistance. Laser cladding process was identified as the best processing technique when compared to processes such as plasma arc, TIG, MIG, etc.

Chapter 3 Research methodology

This chapter presents a detailed description of the raw materials and methodological steps that were developed for laser cladding of Ti-Ni-Nb powder onto titanium alloy (Ti6Al4V) substrate. The process development includes the preparation of powders, laser cladding process parameters, and the characterization of microstructural and mechanical properties of developed samples.

3.1. Nominal composition of powders used

Elemental powders of pure nickel (99.7%), pure titanium (99.6%) and pure niobium (99.5 %) with particle size ranging from 45 µm - 90 µm were used as the starting materials. Both titanium and nickel powders were supplied by TLS Technik Gmbh supplier while niobium powder was supplied by Weartech (Pty) LTD.

As-received elemental powders were weighed to achieve the desired nominal compositions presented in Table 3.1. Nb was added incrementally at 0 wt.%, 2.5 wt. %, 5 wt.% and 7.5 wt. % compositions. The specified compositions were used to deposit thick coating layer on Ti6Al4V substrate.

Table 3.1 : Chemical compositions of the powders in weight percentage.

	wt%.Ti	**wt%.Ni**	**wt%.Nb**
Alloy 1	55	45	0
Alloy 2	53.75	43.75	2.5
Alloy 3	52.5	42.5	5
Alloy 4	51.25	41.25	7.5

3.2. Blending and characterization of powders

Weighed powder mixtures with nominal compositions, were enclosed in small plastic containers, and mixed using a Tubular T2F mixer. The mixer was set at a speed of 300 rpm for a duration of 12 hrs to produce a homogeneous mixture. The advantage of using a tubular mixer was to ensure that the powder particle sizes remained the same.

The morphology of mixed powders was assessed and characterised using a Scanning Electron Microscope (SEM). Figure 3.1 shows the morphology of $Ti_{51.25}Ni_{41.25}Nb_{7.5}$. The powder particles were spherical in shape and homogenously spread.

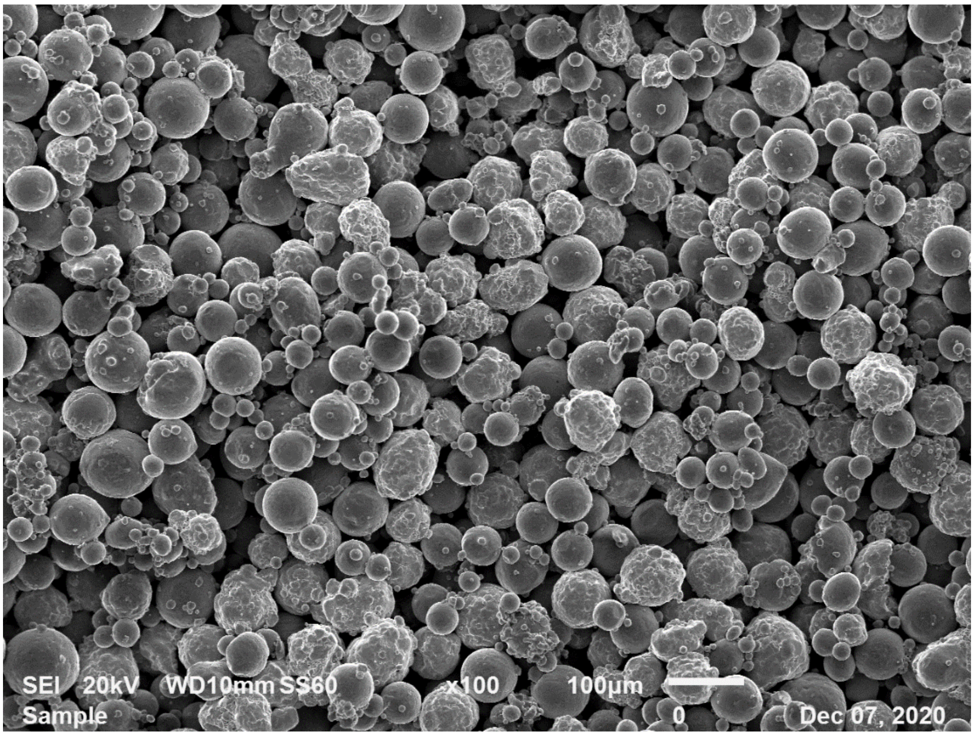

Figure 3.1: Powder morphology of $Ti_{51.25}Ni_{41.25}Nb_{7.5}$

3.3. Laser cladding process

An IRE-Polus Group (IPG) fibre laser with 1073 nm wavelength, 150 mm collimator, 200 µm fibre core and 300 mm lens was used for melting a stream of powder particle to create a good metallurgically bonded coating on Ti6Al4V substrate. The laser was set to laser cladding mode by defocusing a laser beam from an in-focus keyhole mode to give a 2 mm laser beam diameter. Powder efficiency was achieved by aligning laser beam to the centre of a 3-way nozzle (Figure 3.2) mounted on a KUKA robot.

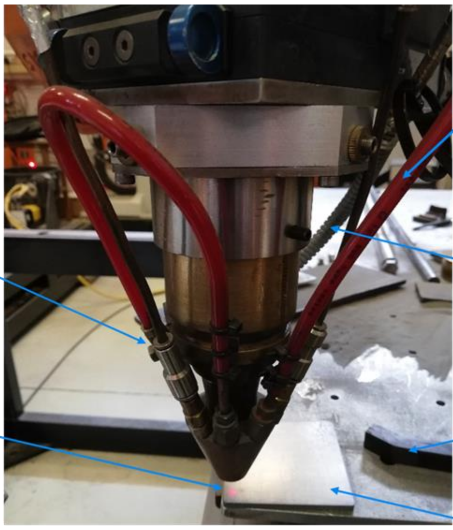

Figure 3.2: Laser cladding nozzle (3-way nozzle).

Prior to laser cladding, the plate was sandblasted to remove possible oxides or rusting, then cleaned with acetone to remove contaminations such as oil and stains caused by cutting fluids which might introduce porosity or cracking during solidification of the clads.

Laser processing was performed at a standoff distance of 12 mm over commercial Ti6Al4V plate with the dimensions 50 × 50 × 5 mm. Molten metal was achieved by laser melting the injecting stream of mixed powder particles to produce a clad width ranging between 2 -3 mm and a clad thickness ranging between 0.65-1.55 mm measured with Olympus BX51M Optical Microscope (OM).

Process development included fabrication of single clads and double clads, and thereafter, full coating (multiple clad) set at 50% clad overlap were fabricated. Figure 3.3 shows the single, double and the multiple clads that were produced.

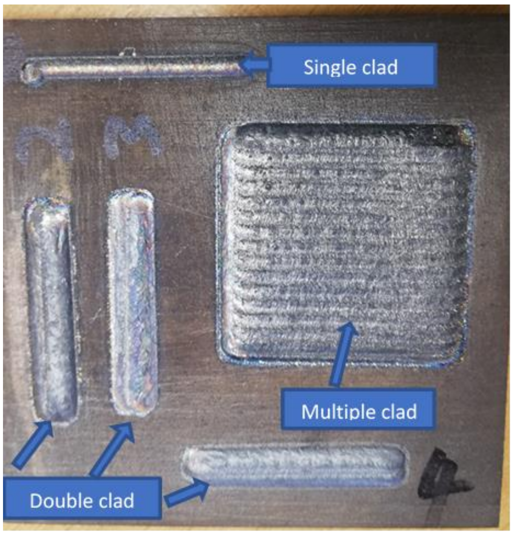

Figure 3.3: Single and multiple clads of Ti-Ni powder laser coated on Ti6Al4V

The laser deposition was scanned in two directions using a KUKA robotic arm positioning system; an argon shielding gas was blown at a flow rate of 12 l/min over the weld pool to prevent oxidation.

3.4. Process parameter optimisation

3.4.1. Powder flow rate development

Powder flow rate was determined by weighing the amount of powder flowing out of the three-way nozzle per minute. This was achieved by injecting powder at a feed rate of 2 rpm for 3 minutes with the carrier gas (argon) flow rate set at 2L/min. The deposition mass per minutes was 14 grams /minutes. The powder flow process was repeated three times to minimize errors. This process helps in determining the amount of powder melted per minute and in determining the cost of powder needed to refurbish components.

3.4.2. Laser parameter development

3.4.2.1. Single clad parameter optimisation process

First part of laser parameter development was determined by producing single clad of Ti-Ni alloy by varying laser power and laser scanning speed using 2 mm beam laser beam diameter at fixed powder feed rate of 2 rev/min, with carrier gas flow rate of 2 L/min and shielding gas flow rate fixed at 12 L/min as shown in Table 3.2

Table 3.2: Laser process parameters optimisation for single clad and double clads using Ti-Ni alloy.

Single clad	Double clad	Laser power (W)	Laser speed (m/min)	Powder feed rate (rev/min)
Sample 1	Sample a	600	0.5	2
Sample 2	Sample b	600	1	2
Sample 3	Sample c	1000	0.5	2
Sample 4	Sample d	1000	1	2

3.4.2.2. Sample production

Optimum laser parameters achieved from laser parameter optimisation in Table 3.2 was used for production of Ti-Ni-Nb alloy samples in Table 3.3.

Table 3.3: Laser parameters for multiple clads of $Ti_{55}Ni_{45}$, $Ti_{53.75}Ni_{43.75}Nb_{2.5}$, $Ti_{52.5}Ni_{42.5}Nb_{5}$ and $Ti_{51.15}Ni_{41.15}Nb_{7.5}$ alloys.

Powder mixture	**Label**	**Laser power (W)**	**Laser scanning speed (m/min)**	**Powder feed rate(rev/min)**
$Ti_{55}Ni_{45}$	Sample a & e	600 & 1000	0.5	2
$Ti_{53.75}Ni_{43.75}Nb_{2.5}$	Sample b & f	600 & 1000	0.5	2
$Ti_{52.5}Ni_{42.5}Nb_{5}$	Sample c & g	600 & 1000	0.5	2
$Ti_{51.25}Ni_{41.25}Nb_{7.5}$	Sample d & h	600 & 1000	0.5	2

3.5. Material characterisation

Metallographic samples were sectioned from clads across the scanning direction using cutting machine. The sectioned pieces were hot mounted in black thermosetting Bakelite resin and thereafter ground with SiC grinding paper using water as a cooling medium. Samples were prepared following the grinding sequence roughness of the grinding grit paper which were from 240, 320, 600, 800 to 1200 grit size.

After grinding, the samples were polished on Struers TegraForce-5 auto/manual polisher to a mirror finished surface of 0.04 µm using the Med-Chem polishing cloth size ranging from 9 µm, 6 µm, 3 µm and 0.04 µm using diamond suspension liquid. Thereafter sample were etched in Kroll's reagent (a mixture of 6 ml nitric acid, 2 ml hydrofluoric acid and 92 ml distilled water) by immersing the samples for approximately 10 seconds.

3.5.1. Optical and scanning electron microscope

The microstructure of produced clads were characterised by using Olympus BX51M Optical Microscope (OM) and Jeol JSM 6510 Scanning Electron Microscope (SEM) with energy dispersive spectroscopy (EDS).

3.5.2. X-ray diffraction

X-rays were used to identify phases present in the produced clads. XRD (XPERT PRO Analytical Netherland) that uses Cu kα radiation (λ = 0.1545 nm). Voltage and current were set at 45 kV and 40 mA respectively. X-ray patterns were scanned over a 2θ ranging from 10° - 90°. XPert Highscore software was used to analyse the patterns obtained from the XRD scans.

3.5.3. Differential scanning calorimeter (DSC)

Differential Scanning Calorimeter (DSC) NETZSCH's STA 449 F3 Jupiter®) model was used to determine the transition temperatures within the sample clads. This was accomplished by heating the samples from room temperature to 1200°C and then cooled to 40°C. The heating and cooling rates were set at 10K/min.

3.6. Mechanical testing

The two mechanical tests that were performed on the clads, are wear and hardness tests.

3.6.1. Wear testing

Wear test was performed by using Tribometer version 7.3.13 using ball on disc technique. A 6 mm steel ball pin was applied to the coating surface. A load of 5N was applied to the samples at sliding stroke speed of 24.42 cm/s for a duration of 25 minutes. A load of 5N was determined after analysing surface tracks of three different loads (3N, 4N and 5N) applied on Ti-Ni clad surface for 1min at 24.42cm/s sliding stroke. Visible sliding tracks were observed at 5N than at 3N and 4N loads.

Tribometer instrument was used to measure the coefficient of friction (COF), friction force and the wear volume between the two contact surfaces. The experiments were done without lubrication. Prior to testing, the steel ball and the sample surface were cleaned with acetone to remove oil residue or contaminants that might affect the results.

3.6.2. Hardness testing

Hardness measurement of the coating were taken in the transverse direction, from the top of the clad through heat affect zone and unaffected parent material area. Zwick Vickers microhardness tester (Figure 3.4) situated at NLC/CSIR was used to measure the hardness of the coating. Tests were performed using a load of 500g, the spacing between indentations was set at 548μm, and the dwell time of 10 sec was applied. About 11 indentations were taken across the longitudinal direction of the sample.

Figure 3.4: Vickers micro-hardness machine

3.7. Summary of Chapter 3

This chapter provides the methodological steps of equipment used, the chemical composition and the powder mixing technique used, it also provides steps used for process development which includes laser cladding process and characterisations of coating.

Chapter 4 Results and Discussion

This chapter presents results and discussion of characterised clad produced by laser deposition of mechanically pre-alloyed powders. The composition of the powders consisted of pure niobium (99.5%Nb), pure nickel (99.7%Ni) and pure titanium (99.6%Ti). Clads were produced by varying and laser scanning speed at a fixed laser beam diameter. Clads characterisations results included optical microscopic (OM), SEM with EDS and X-ray analyses. The DSC and mechanical properties results are also included in this chapter.

4.1. Single clads

Single clads were produced under varying conditions to determine the optimum laser parameter for Ti-Ni alloy prior to the addition of niobium. Figure 4.1 shows single clad tracks corresponding to process parameters presented in Chapter 3 in Table 3.1.

Figure 4.1: Singe clads of Ti-Ni alloy, sample 1 produced at 600w with 0.5m/min, (2) at 600w with 1m/min, (3) at 1000w with 0.5m/min and (4) produced at 1000w with 1m/min.

Sample 1 shown in Figure 4.1 had good bonding with light grey colour and a combination of rough and smooths surface. However, sample 2 had a fully rough surface, with unmelt powder particles on the surface of the clad. This was an indication that the heat input, which is the combination of laser power and laser scanning speed was insufficient to produce a fully melted clad compared to samples 1, 3 and 4.

Sample 3 had the thickest and widest clad of all samples. This sample was produced when the laser power was set at 1000W and laser scanning speed of 0.5m/min. This observation affirmed that higher heat input melts more powder resulting in a thicker clad. Sample 4 had a shiny smooth surface, with less clad thickness than that of sample 3. This sample was produced at same power as sample 3 but at faster laser scanning of 1m/min. After metallographic preparations, samples were analysed under the microscope to evaluate the resulting microstructures and analyse macro defects that might have formed during production of clads. Optical micrographs of Ti-Ni single clads produced by varying laser power and laser scanning speed are presented in Figure 4.2.

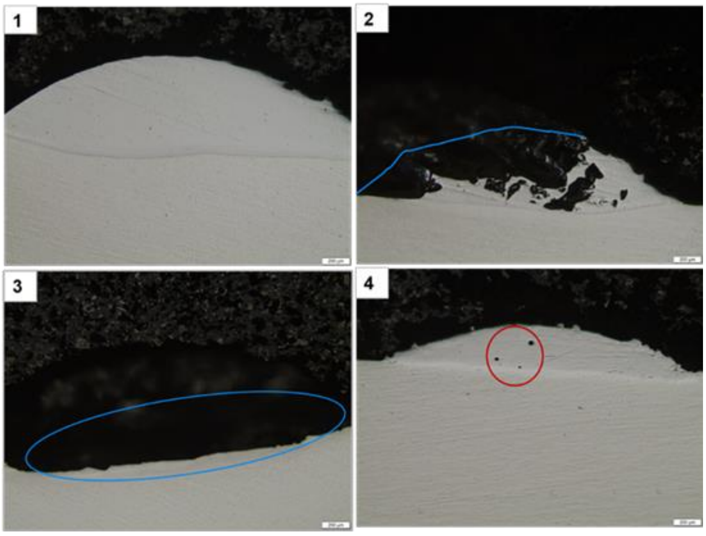

Figure 4.2: Optical micrographs of Ti-Ni single clads produced at varying laser power and scanning speed (1) 600W and 0.5m/min, (2) 600W and 1m/min, (3) 1000W and 0.5m/min, (4) 1000W and 1m/min.

Sample 1 clad in Figure 4.2 shows a good, fully bonded clad with no defects. Sample 2 partly delaminated during metallographic preparation. This shows that the clad was not fully fused onto the substrate. Sample 3 also delaminated as indicated with the blue circle. This sample was produced using high laser power of 1000W and slower scanning speed of 0.5m/min. High laser power and lower scanning speed causes high heat input which result with high dilution.

High dilution promotes diffusion of base metal elements into the clad. If more titanium diffused into the clad, the Ti_2Ni phase form according to the Ti-Ni phase diagram. The Ti_2Ni

intermetallic phase which is hard and brittle forms when Ti composition is above 55 wt% [1]. However, brittle materials are crack sensitive [7] .

Sample 4 shows thin clad with low dilution. This sample had black spots, highlighted in a red circle, on the surface that are synonymous with gas bubble pores in laser cladding. Good fusion and high dilution were observed when laser power increased from 600W to 1000W, whereas, increasing the laser scanning speed from 0.5m/min resulted in less dilution and thinner clad thickness on clads produced at 1000W.

4.2. Multiple clads optical analysis

Figure 4.3 present double clads produced at 50% overlap. Double clads were produced to check the effect of induced heat to metallurgical bonding of the clad and dilution.

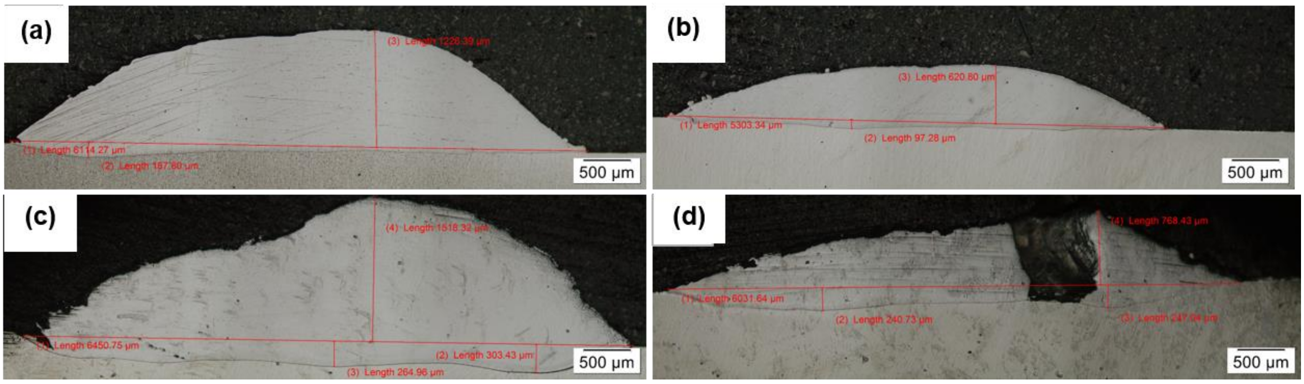

Figure 4.3: Multiple clads of Ti-Ni alloy with sample (a) produced at 600W at 0.5m/min, (b) 600W at 1m/min, (c) 1000W at 0.5m/min and (d) 1000W at 1m/min.

Clad thickness and dilution were measured using Equation 2, and the results are presented in Table 4.1. Ideal laser process parameters produce clads that are crack free, with less dilution and at least have a thickness above 1 mm for easy characterisation.

$\text{Percent dilution} = \frac{HD}{HC+HD)} * 100$ ………………………………………… Equation 2 [11].

Where HD is a depth of the dilution and HC is the thickness of the coating.

Table 4.1: Dilution for the multiple clads of Ti-Ni alloy with sample (a) produced at 600W at 0.5m/min, (b) 600W at 1m/min, (c) 1000W at 0.5m/min and (d) 1000W at 1m/min

	Process parameters	**Dilution(mm)**	**Clad thickness(mm)**	**% Dilution**
Sample (a)	600 W & 0.5m/min	0.168	1.226	12.05
Sample (b)	600 W & 1m/min	0.0972	0.621	13.7
Sample (c)	1000 W & 0.5 m/min	0.303	1.518	16.6
Sample (d)	1000 W & 1m/mi	0.247	0.768	24.3

The clad thickness of sample (a) in Figure 4.3 was 1.226 mm with 12% dilution. Sample (b) measured approximately the same dilution but with 50% less coating thickness, while sample (c) measure about 16.6% dilution and sample (d) measured about 24.3% dilution. The observed results agreed with observation by Ali et al. [11] where they observed increases in dilution and clad thickness with increase in heat input.

From optical microscope analysis of multiple clads, sample (b) produced at 600W, and 1m/min was eliminated due to its thinner coating and poor fusion, while sample (d) was eliminated due to high dilution and thinner clad thickness. High dilution cause more of the base composition element to diffuse into the clad which can affect the Ti/Ni ratio and result in the formation of Ti_2Ni intermetallic. Shallow thickness delaminated easily from the base material and therefore not easy to characterise. Less dilution and thicker clad were the main factor in achieving and identifying optimum parameters. These optimum conditions were observed on sample (a). Although sample (c) had high dilution, but it had good fusion and enough clad thickness for easy characterisation.

4.3. Optical microscope results of $Ti_{50-x/2}Ni_{50-x/2}Nb_x$

Clads analysed at this stage were clads with added niobium. After optical microscopic observation of the full clads analysed using polarized light, optical micrographs were snapped at the top and bottom of the clad to check for homogeneity of the structure throughout the clad.

4.3.1. Optical micrographs of Ti50-x/2 Ni50-x/2Nbx produced at 600W laser power and 0.5m/min laser scanning speed

Figure 4.4 (a)-(d) presents optical micrographs of $Ti_{50-x/2}Ni_{50-x/2}Nb_x$ alloys with increasing niobium content. All micrographs were obtained at the centre of the sample/clad using 1000X magnification.

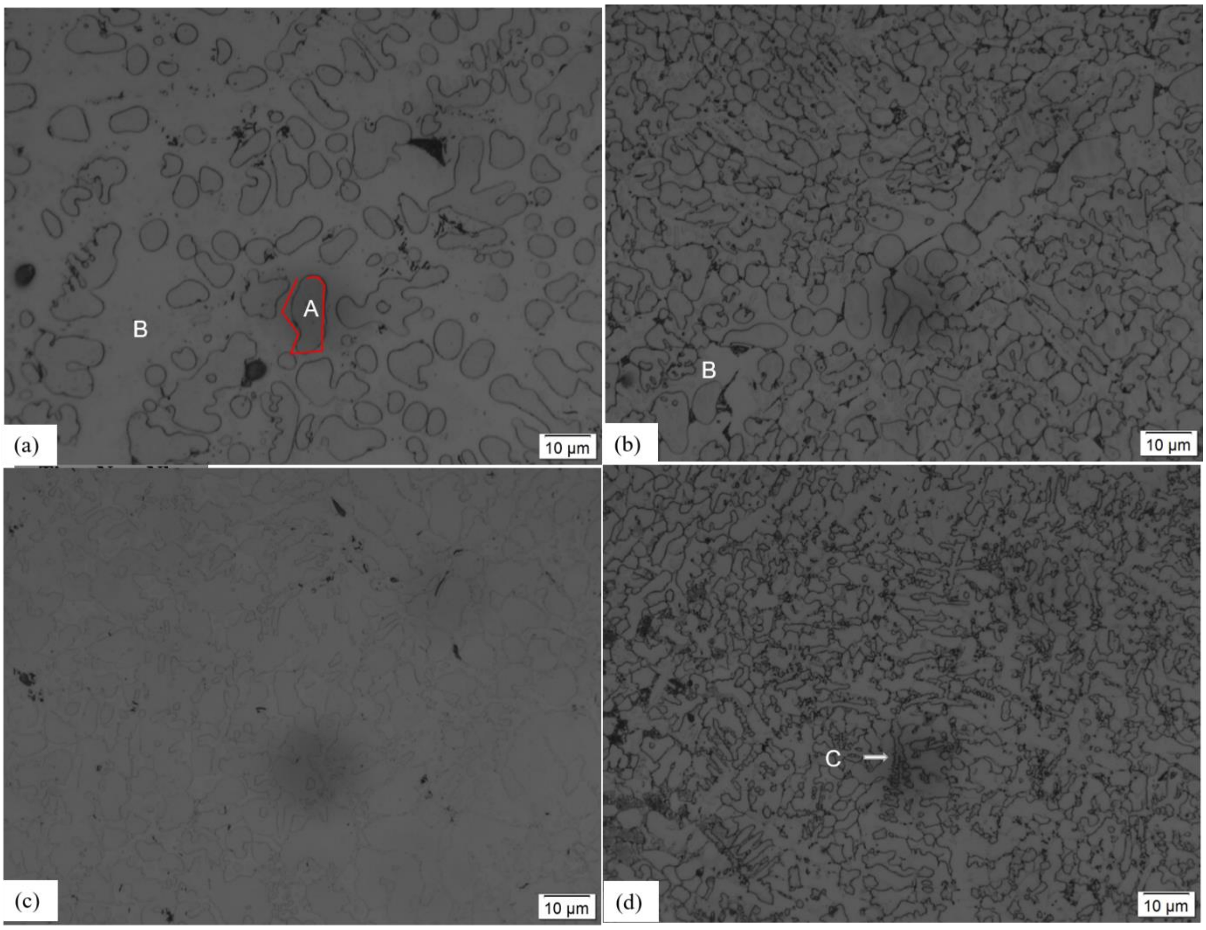

Figure 4.4: Optical micrographs of (a) $Ti_{55}Ni_{45}$, (b) $Ti_{53.75}Ni_{43.75}Nb_{2.5}$ (c) $Ti_{52.5}Ni_{42.5}Nb_5$ and (d) $Ti_{51.15}Ni_{41.15}Nb_{7.5}$ produce at 600W laser power and 0.5m/min laser scanning speed.

All microstructures comprise of two distinct phases. Figure 4-4 (a) shows dark-grey globular phase circled in red and labelled "A" which precipitated on a light-grey matrix labelled "B".

The phase labelled "B" was confirmed using SEM to be $NiTi_2$ and "A" as NiTi. Figure 4-4 (a) microstructure comprises of larger globular phase as compared to finer globular phase in other microstructures. Whereas, Figures 4-4 (b), (c) and (d) microstructures show a mixture of globular and dendritic microstructure. However, Figure 4-4 (d) had finer dendrites than in Figures 4-4 (b) and (c). Since all these clads were produced with a fixed laser power and fixed scanning speed, addition of niobium led to the refinement of the globular structure into fine dendritic structure. A dendritic microstructure was associated with constitutional super-cooling [39].

4.3.2. Optical micrographs of Ti50-x/2 Ni50-x/2Nbx produce at 1000W laser power and 0.5m/min laser scanning speed

Figure 4.5 shows micrographs of samples produced at laser power of 1000W and 0.5m/min scanning speed. Increasing the laser power from 600W to 1000W produced similar microstructural features that were observed when the laser power was set at 600W, but with larger dendrites and much brighter phase.

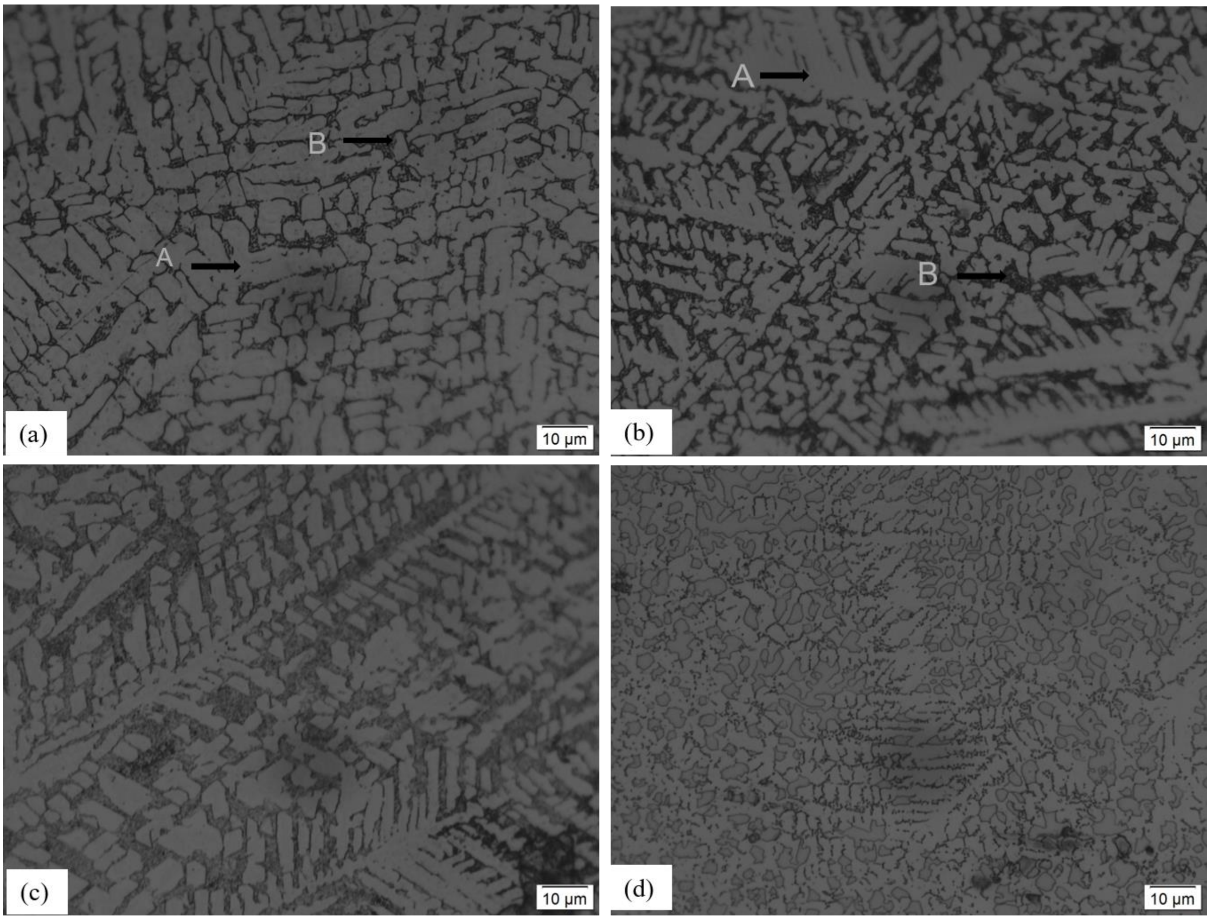

Figure 4.5: Optical micrographs of (a) $Ti_{55}Ni_{45}$, (b) $Ti_{53.75}Ni_{43.75}Nb_{2.5}$ (c) $Ti_{52.5}Ni_{42.5}Nb_5$ and (d) $Ti_{51.15}Ni_{41.15}Nb_{7.5}$ produce at 1000W and 0.5m/min

Figure 4-5 (a) shows optical micrographs of alloys produced at 1000W laser power and 0.5 m/min scanning speed. All sample contained brighter phase labelled "A" and grey matrix labelled "B" that were analysed in EDS section. Brighter colours were analysed as titanium rich phase which might come during diffusion of titanium from the base due to high dilution. Samples (b) and (c) has dendritic microstructure with light and grey phase that were reported by Abioye et al. [21]. Sample (d) showed finer dendrite and globular structure.

Figure 4-6 presents micrograph of sample produced at 1000W and a scanning speed of 0.5m/min. The image was obtained near the edge of the clad. The samples showed more cracks towards the edges.

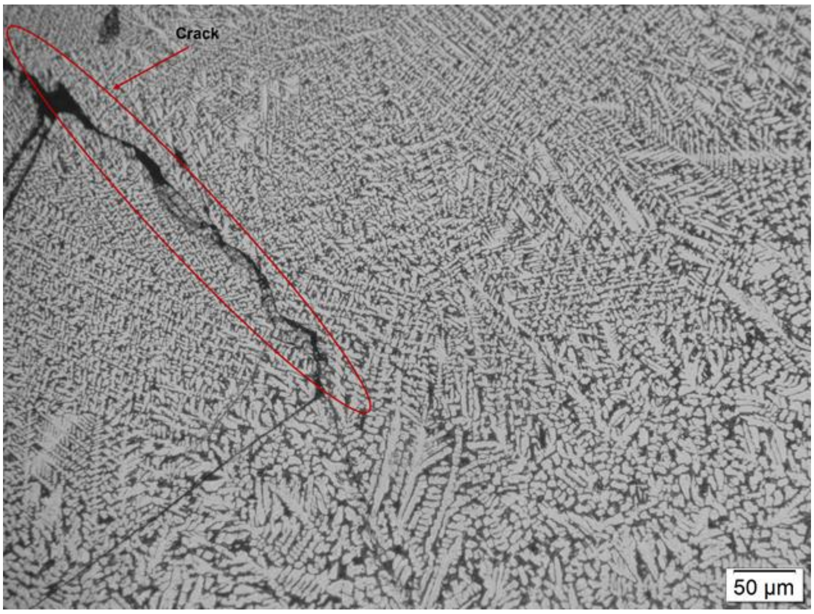

Figure 4.6: Optical micrographs of $Ti_{53.75}Ni_{43.75}Nb_{2.5}$ produced at laser power of 1000W and 0.5m/min scanning speed.

Cracking might result from rapid solidification rate occurring at the toes of the clad, and it might be due to the presence of Ti_2Ni intermetallic phase which is brittle and crack sensitive [1, 7]. High laser power and slow scanning speed parameters produced high dilution, high dilution of titanium alloy base has titanium rich interface [6], and titanium rich has Ti_2Ni intermetallic phase, rapid cooling of the titanium rich region produced martensitic structure with residual stress that might have resulted in cracking.

4.4. SEM and Energy dispersive spectroscopy results of the coating

Figure 4-7 presents the EDS results of $Ti_{55}Ni_{45}$ clad produced at 600W using 0.5 m/min scanning speed, and the chemical composition of the sample were measured using the SEM coupled with EDS. Random chemical compositions were taken on each phase, and three spots were measured on each phase.

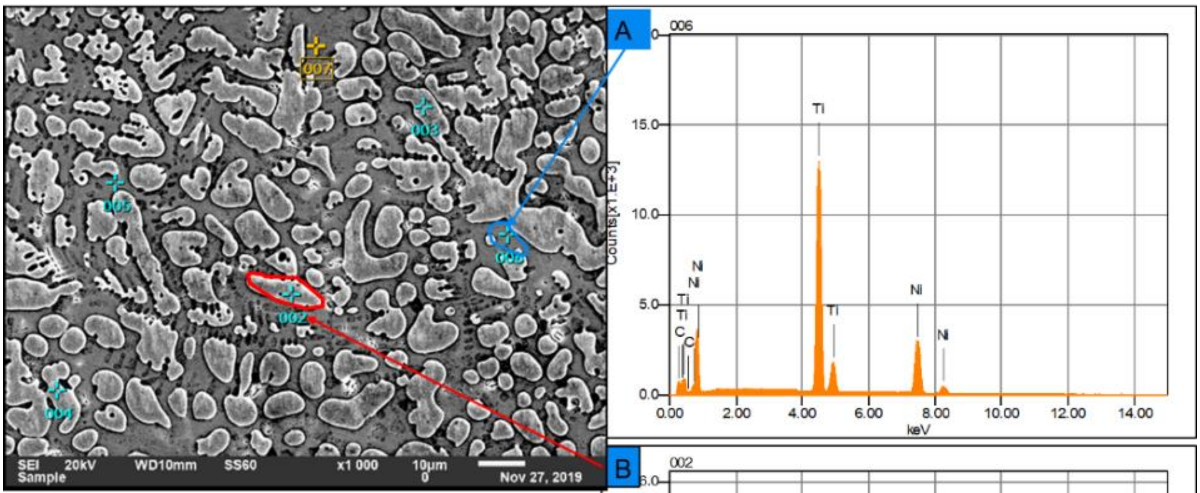

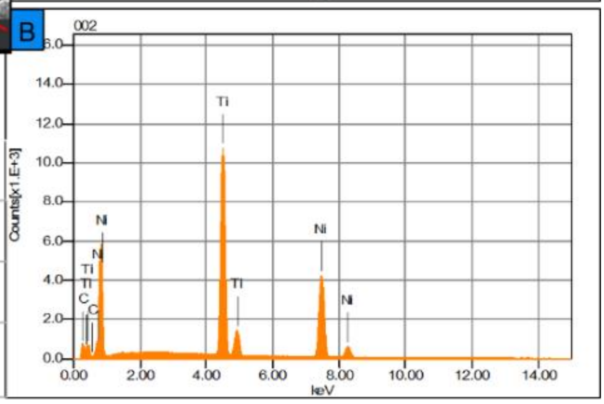

Atomic %			
EDS point	Ti %	Ni %	Intermetallic
A	55,65	30,88	$NiTi_2$
B	43,89	40,47	NiTi

Figure 4.7: EDS analysis of $Ti_{55}Ni_{45}$ produced at 600W with 0.5m/min

A globular light grey phase circled in red, in Figure 4-7, contained approximately equal atomic percent of Ti and Ni. This phase was found to correlate with NiTi intermetallic. The dark-grey matrix, circled in blue, contained Ti and Ni in the atomic ratio of 1:2, which correlated with $NiTi_2$ intermetallic composition

Figure 4.8 shows the EDS spectrum of $Ti_{51.15}Ni_{41.15}Nb_{7.5}$ sample, the EDS spots were measured at different areas of the microstructure. At least four EDS spots were measured on the grey area and five EDS spots on the dark dendritic area.

	Atomic % of elements			
EDS spots	Ti%	Ni%	Nb%	Intermetallic
002	40.46	48.92	0.87	NiTi
003	39.79	38.42	0.74	NiTi
004	39.52	38.14	0.71	NiTi
005	45.14	22.81	0.11	$NiTi_2$
006	40.46	32.25	4.43	Ti_3Ni_4
007	43.18	22.04	8.25	$NiTi_2$
008	42.72	26.5	6.11	$NiTi_2$
009	50.15	26.59	2.94	$NiTi_2$
010	47.87	29.50	2.57	Ti_3Ni_5

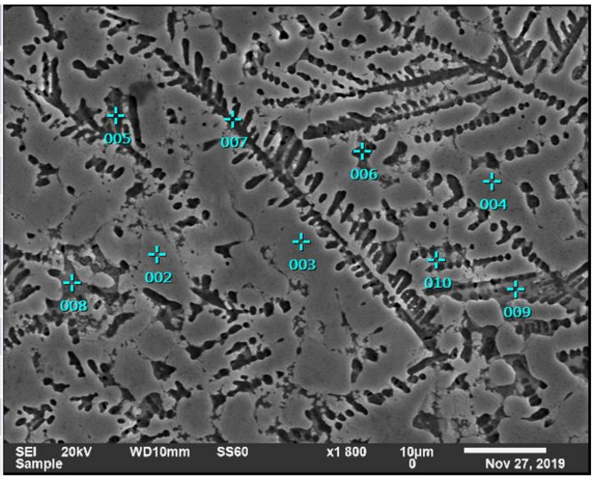

Figure 4.8: Overall EDS spectrum of $Ti_{51.15}Ni_{41.15}Nb_{7.5}$ produced at laser power of 600W and 0.5m/min laser scanning speed.

The EDS spots 002,003 and 004 had approximately 1:1 atomic ratio of (Ti/Ni). This suggests that the grey area relates to NiTi, and the dark area is associated with $NiTi_2$, Ti_3Ni_4 and Ti_3Ni_5. It was observed that as the niobium addition increase, the microstructure changed from globular structure to dendritic microstructure, and it was also noticed that an increase in niobium content led to an increase in the amount of grey phase, which was confirmed as NiTi.

4.5. SEM microstructural analyses of $Ti_{50-x/2}Ni_{50-x/2}Nb_x$ alloys

Figure 4.9 presents the SEM microstructures of $Ti_{55}Ni_{45}$, $Ti_{53.75}Ni_{43.75}Nb_{2.5}$, $Ti_{52.5}Ni_{42.5}Nb_5$ and $Ti_{51.15}Ni_{41.15}Nb_{7.5}$ for samples produce at laser power of 600W when the scanning speed was set at 0.5m/min.

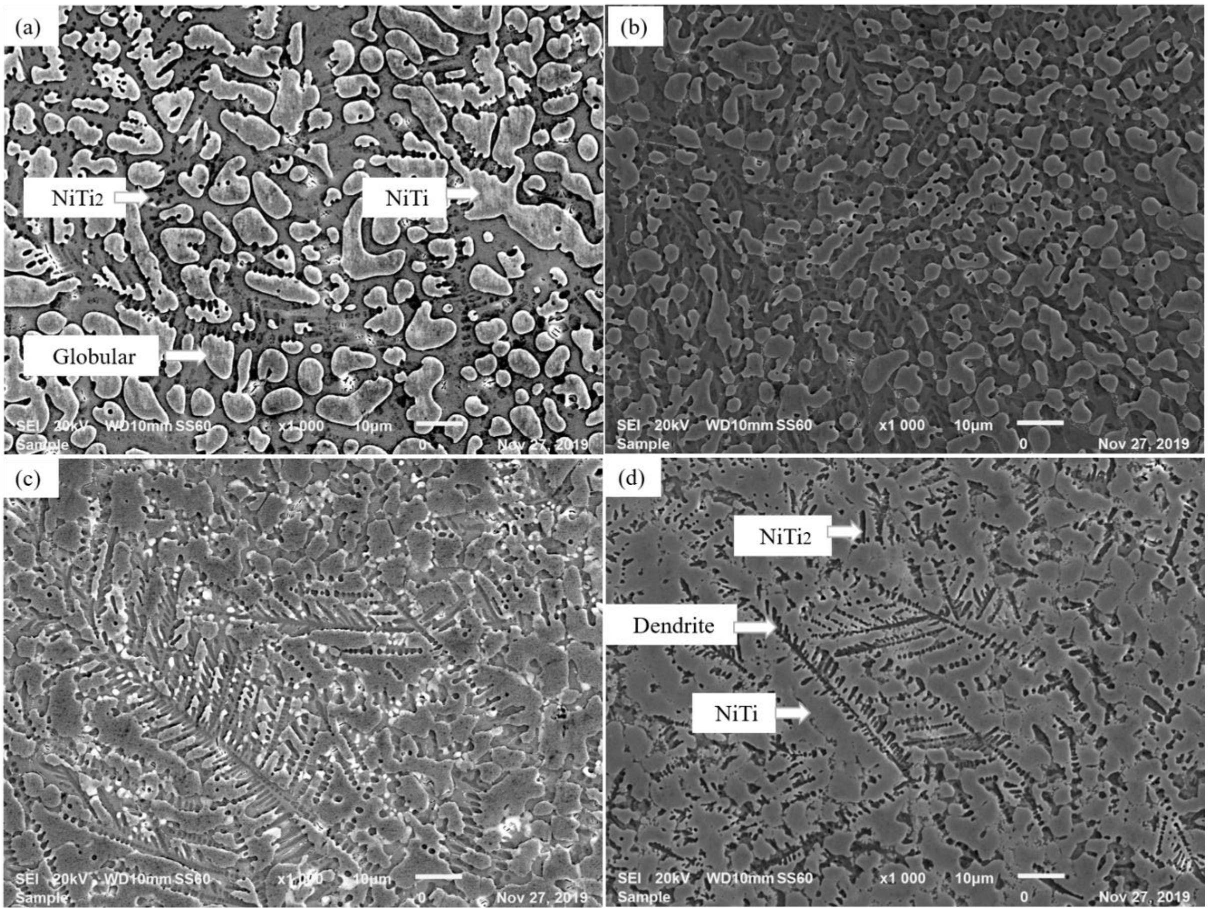

Figure 4.9: SEM micrographs of four typical $Ti_{50-x/2}$ $Ni_{50-x/2}Nb_x$ alloys: (a) $Ti_{55}Ni_{45}$, (b) $Ti_{53.75}Ni_{43.75}Nb_{2.5}$ (c) $Ti_{52.5}Ni_{42.5}Nb_5$ and (d) $Ti_{51.15}Ni_{41.15}Nb_{7.5}$ produced at 600W and 0.5m/min

The SEM micrographs of Figures 4.9 (a) and (b) show a mixture of globular and dendritic microstructure. The dendrites were not clearly visible under the optical microscope. Light grey globular phase was found to be NiTi, and a dark-grey matrix was related with $NiTi_2$. These findings were confirmed by EDS composition analysis in Figure 4.7. The effect of Nb addition was clearly noticeably by formation of clear fine dendrite in Figure (c) and (d). The $NiTi_2$ phase was obtained within the dendrite while NiTi intermetallic was found within the grey matrix. As the content of Nb addition increased, the amount of $NiTi_2$ phase decreased while the amount of NiTi increased. Zhang et al. [7] also observed that the precipitation size of Ti_2Ni decreases with an increase in niobium addition.

4.6. XRD results $Ti_{50-x/2}Ni_{50-x/2}Nb_x$ alloys

The XRD analyses were conducted to investigate phase transformation changes that occurred due to the addition of niobium and to check the crystallinity of the structure. The XRD diffraction graphs obtained for different $Ti_{50-x/2}$ $Ni_{50-x/2}Nb_x$ alloy produced at laser power of 600W and 0.5m/min laser scanning speed are shown in Figure 4.10.

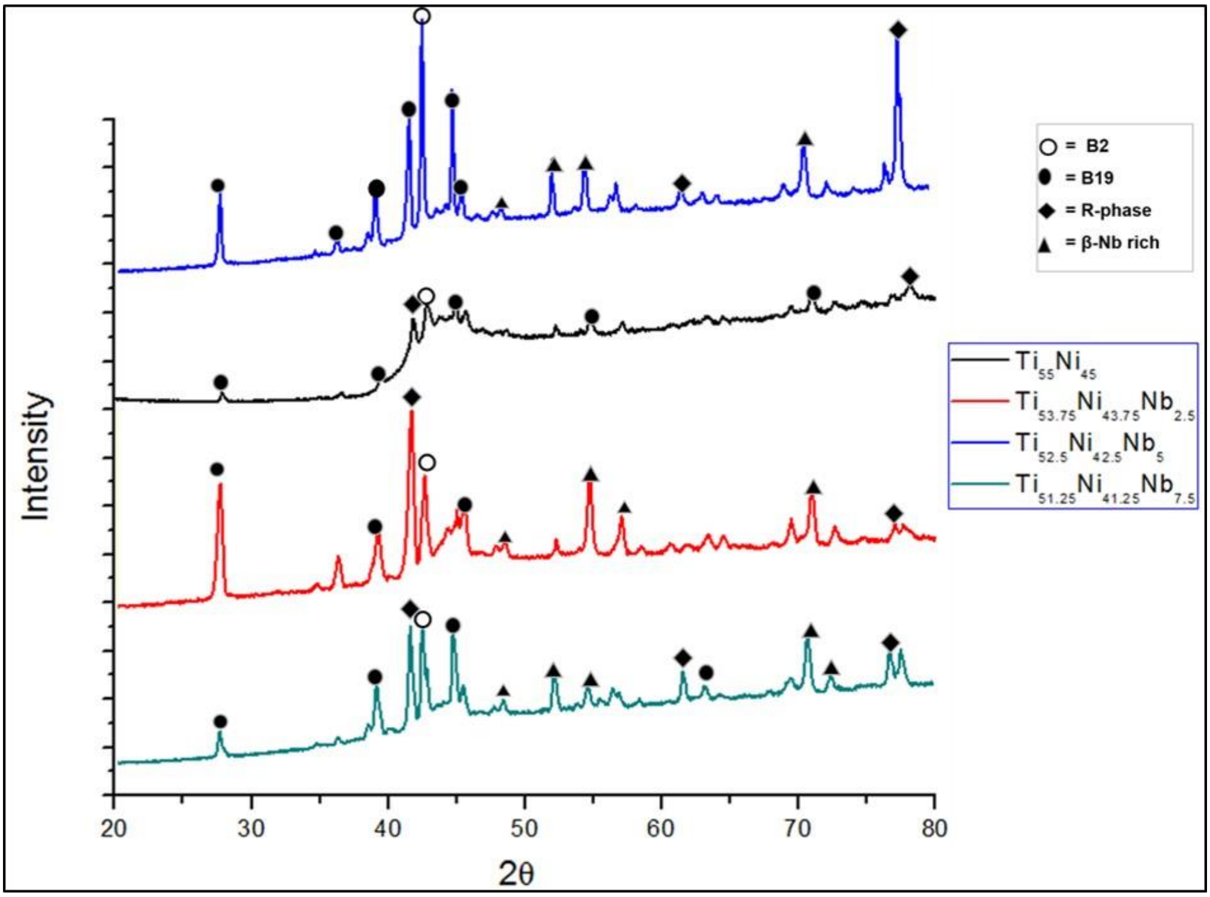

Figure 4.10: XRD pattern of $Ti_{55}Ni_{45}$, $Ti_{53.75}Ni_{43.75}Nb_{2.5}$, $Ti_{52.5}Ni_{42.5}Nb_5$ and $Ti_{51.15}Ni_{41.15}Nb_{7.5}$ produced at laser power of 600W and scan speed of 0.5m/min

The XRD spectrum in Figure 4-10 show B2 (austenite), B19 (martensitic), R-phase (rhombohedral) and niobium rich phase. The XRD peaks for austenite phase were related to the reference data from ICDD standard 35-1281, and the martensitic XRD peaks were referenced using ICDD standard 18-0899, while R-phase was compared to the calibrated data by River et al. [28], and niobium rich peaks observed, were correlated to XRD data reported by Cronemberger et al. [8]. The addition of niobium did not change the original position of B19 (martensitic) and B2 (austenitic) phases but increased the intensity of these peaks.

The increase in intensity with addition in Nb was also observed by Li et al. [40]. XRD However, at 7.5 wt.%Nb, R-phase, which is normally present at 2θ values of 42.2° and 42.7° disappeared. The disappearance of R-phase was also observed by Zhang et al. [7]. The XRD patterns for $Ti_{55}Ni_{45}$ alloy exhibited poor crystallinity with low peak intensity. With addition of niobium, the intensity of the peaks was seen to be increasing. The SEM result in Figure 4-9 showed increase in NiTi phase, and decrease in Ti_2Ni with increase in Nb addition, the same trend was observed with XRD patterns for NiTiNb alloy, the intensity peaks for NiTi (B2 and B19) phase increased with increase with Nb addition.

4.7. Differential Scanning Calorimeter results

Differential scanning calorimeter results were measured using NETZSCH's STA 449 F3 Jupiter® to relate the transition temperature with the phases observed from XRD analyses. The two samples that were examined are $Ti_{55}Ni_{45}$ (Sample (a) and $Ti_{51.25}Ni_{41.25}Nb_{7.5}$ alloy (Sample (d)) produced at laser power of 600W and 0.5m/min laser scanning speed. Figure 4.11 presents the DSC heating and cooling curves for $Ti_{55}Ni_{45}$ alloy (Sample a).

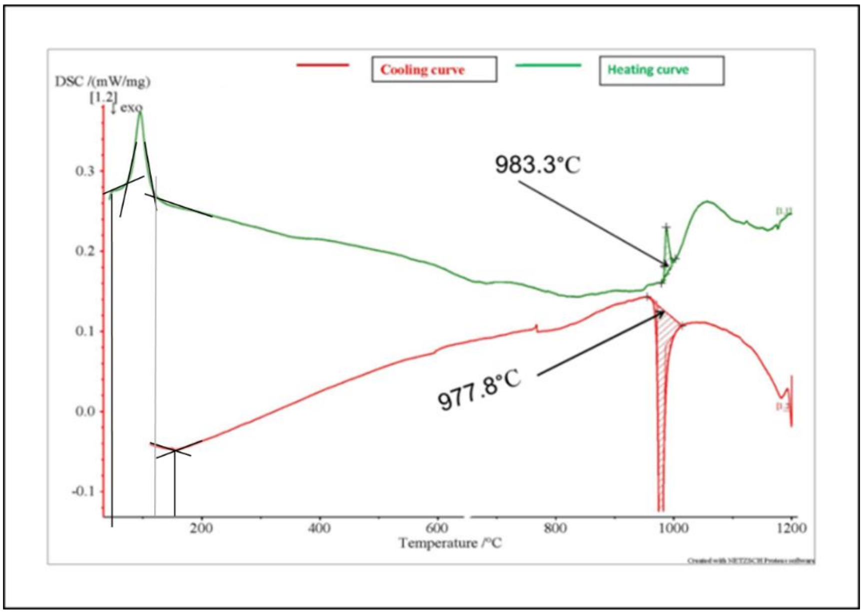

Figure 4.11: DSC curve of $Ti_{55}Ni_{45}$ sample produced at 600W laser power and 0.5m/min scanning speed

The start and finish of austenite and martensitic were determined by plotting tangential lines on the graphs as seen on Figure 4.11. The heating curve (green line) shows an endothermic peak at 19°C, the peak was related to austenitic start (A_s). This peak was observed at approximately the same temperature as the A_s at 20°C reported by to Cronemberger et al. [8].

The austenitic finish (A_f) temperature was observed at 120°C, this transition differs to A_f = 39°C reported by Cronemberga et al. [8] and differs to A_F = 95.6°C reported by Chan et al. [29]. The endothermic peak (green line) observed at 983.3°C was related to a reaction of $\mathrm{NiTi(s) + NiTi_3(s) \rightarrow 3NiTi}\ (s)$, this reaction occurs at 984°C according to the Ti-Ni phase diagram [24]. The cooling curve (red line) shows eutectoid reaction producing exothermic peak at 977.8°C, $NiTi\ (s) \rightarrow NiTi\ (s) +\ NiTi_3(s)$.

The DSC heating and cooling curve for $Ti_{51.25}Ni_{41.25}Nb_{7.5}$ alloy are presented in Figure 4.12.

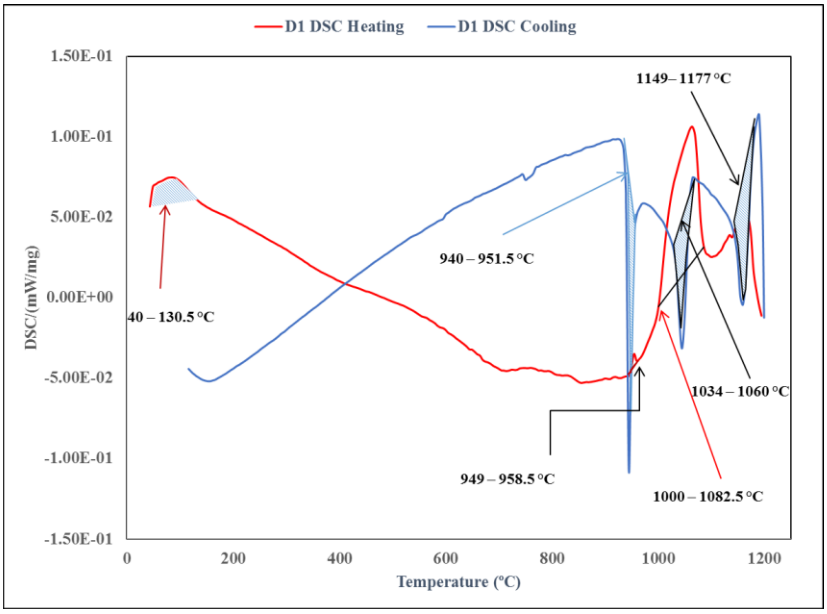

Figure 4.12: Heating and cooling DSC curve for $Ti_{51.25}Ni_{41.25}Nb_{7.5}$ alloy

The heating curve (red curve) for $Ti_{51.25}Ni_{41.25}Nb_{7.5}$ alloy in Figure 4.12 shows austenitic start at 40°C and austenitic finish at 130.5°C. These values (A_s = 40°C and A_f = 103.5°C) were slightly higher than that of Ni-Ti alloy which are A_s=19°C and A_f =120°C. However, Cronemberger et al. [8], reported a slight decreased in austenitic transformation with niobium addition. The endothermic peak observed at range between 1000°C – 1082.5°C corresponded with $\mathrm{NiTi} \rightarrow L + NiTi_3$ reaction, which normally starts at 1118°C according to the Ti-Ni phase diagram [24].

The cooling curve for $Ti_{51.25}Ni_{41.25}Nb_{7.5}$ alloy in Figure 4.12 exhibits three features. The first peak occurred below 1149°C- 1177°C, the second peak occurred at 1034°C -1060 °C and the third peak occurred at 940°C - 951°C.

The first peak was attributed to a eutectic reaction $L \rightarrow NiTi + NiTi_3$, the second peak was attributed to $NiTi_{3(S)} + \mathrm{L} \rightarrow NiTi_{(S)}$. While the third peak was attributed to $NiTi_{3(S)} + NiTi_{(S)} \rightarrow NiTi_{(S)}$ [24]. The addition of 7.5% Nb in NiTi alloy has slight increased hysteresis, this similar trend was also observed by Polozov et al. [4], were A_f was increased from -5°C to 20°C with 15% addition in Nitinol.

4.8. Hardness results

Figure 4.13 presents hardness results of $Ti_{55}Ni_{45}$, $Ti_{53.75}Ni_{43.75}Nb_{2.5}$, $Ti_{52.5}Ni_{42.5}Nb_5$ and $Ti_{51.15}Ni_{41.15}Nb_{7.5}$ samples produced at 600W and laser scanning speed of 0.5m/min. The hardness measurements of the clad were taken in the transverse direction, from the top of the clad through heat affected zone and unaffected parent material area.

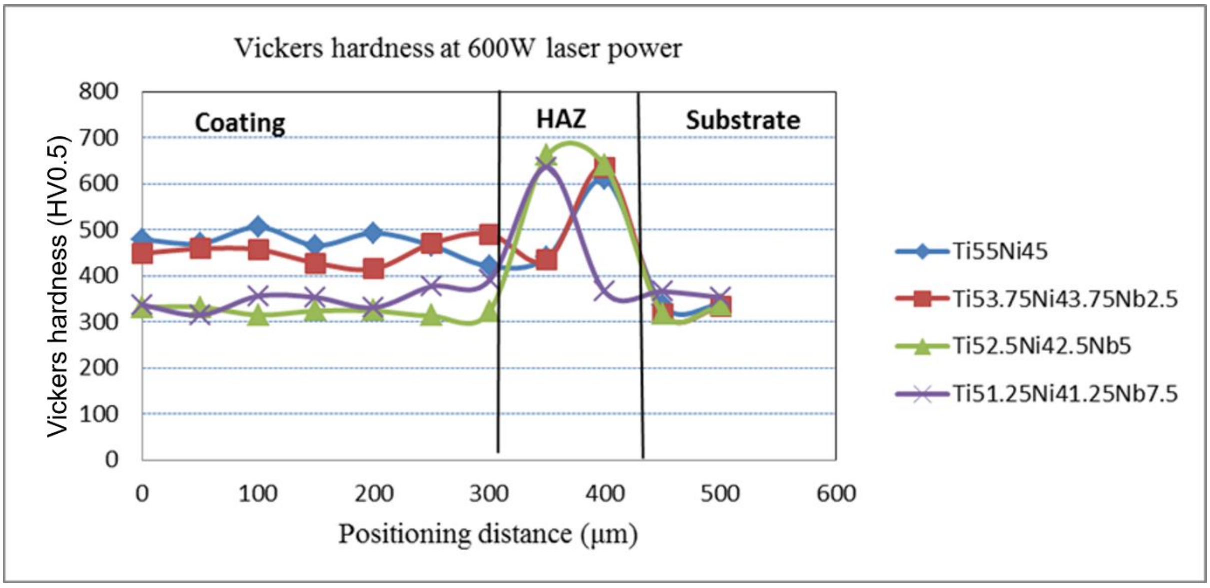

Figure 4.13: Microhardness profile of laser deposited $Ti_{50-x/2}Ni_{50-x/2}Nb_x$ alloy coating

An average of 494 HV was obtained for $Ti_{55}Ni_{45}$ coating higher than the hardness of parent material (Ti6Al4V) of 315 HV. The obtained hardness for $Ti_{55}Ni_{45}$ coating was 30% lower than the hardness reported by Mokgalaka et al. [1]. The low hardness observed could be due to low heat input as compared to high heat input used by Mokgalaka et al. [1]. High laser heat input on Ti6Al4V promoted diffusion of Ti from parent material to the clad which resulted in the formation of $NiTi_2$, Ti_3Ni_4 and Ti_3Ni_5 brittle intermetallics [1]. However, Abioye et al. [21], reported high hardness at interface of laser cladded Ni-Ti alloy on Ti6Al4V substrate, this high hardness was due to formation of $NiTi_2$ intermetallic phase [21].

The addition of about 7.5 wt.% niobium in $Ti_{55}Ni_{45}$ decreased the hardness of $Ti_{55}Ni_{45}$ by 37%. The decrease in hardness was correlated to a decrease in the amount of $NiTi_2$ intermetallic. The $NiTi_2$ intermetallic is more brittle than NiTi intermetallic [1]. All clads showed average hardness of 690 HV at the heat-affected zone than the coating. It is normal to observe high hardness at the heat affected when cooling titanium very fast [37]. Fast cooling from transformation temperature yield grain refinement structure which increases hardness [5].

Figure 4.14 presents the hardness results of $Ti_{55}Ni_{45}$, $Ti_{53.75}Ni_{43.75}Nb_{2.5}$, $Ti_{52.5}Ni_{42.5}Nb_5$ and $Ti_{51.15}Ni_{41.15}Nb_{7.5}$ alloys produced at 1000W laser power and 0.5m/min laser scanning speed.

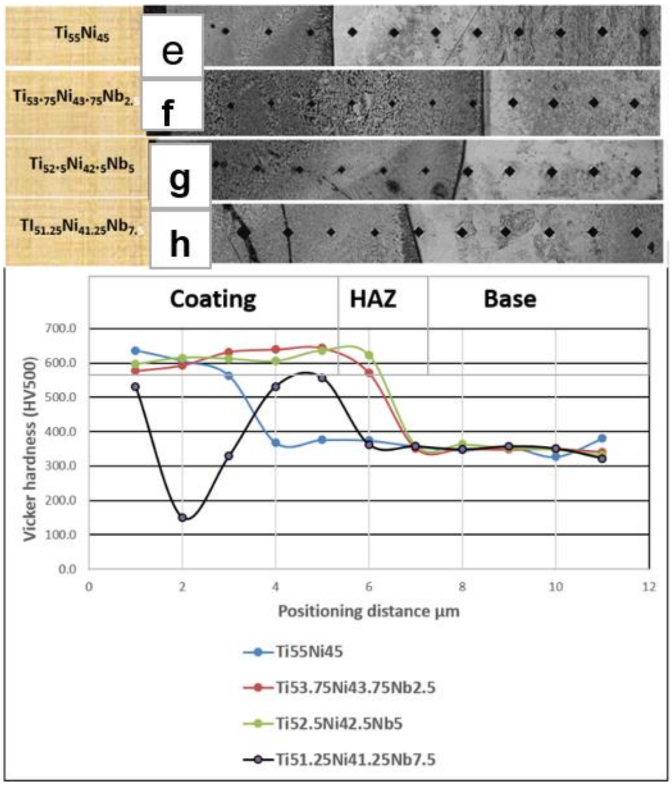

Figure 4.14: Hardness results of $Ti_{50-x/2}$ $Ni_{50-x/2}Nb_x$ alloy samples produced at 1000W laser power and 0.5m/min laser scanning speed.

The coatings on samples (e), (f) and (g) produced at high laser power(1000W) and slow scanning speed (0.5m/min) have an average hardness of about 600 HV, which is 100 HV higher than the hardness of all samples produced at 600W. From the observations, it can be concluded that this higher hardness was due to titanium diffusing from the substrate to the clad, in turn, it formed brittle Ti_2Ni intermetallic phases as results of high heat input. Cracks were observed on the coating of sample (h) which is the evidence of the brittle nature of the microstructure. The coating measured the same hardness as HAZ. The HAZ and clad measuring the same hardness can be an indication of softening of the HAZ. The softening of the HAZ is attributed to slow solidification rate due to high heat input, slow solidification promotes grain growth result in low hardness [37]. These samples experienced higher heat input since they were produced at higher laser power and slow scanning speed.

4.9. Wear test results

Figure 4.15 present coefficient of friction versus time results of $Ti_{55}Ni_{45}$, $Ti_{53.75}Ni_{43.75}Nb_{2.5}$, $Ti_{52.5}Ni_{42.5}Nb_{5}$ and $Ti_{51.15}Ni_{41.15}Nb_{7.5}$ alloy samples produced at fixed laser power of 600W and scanning speed of 0.5 m/min. The wear test was only performed for the sample produce at 600W and laser scanning speed of 0.5m/min because samples produce at 1000W and 0.5m/min formed cracks as seen in Figure 4.6.

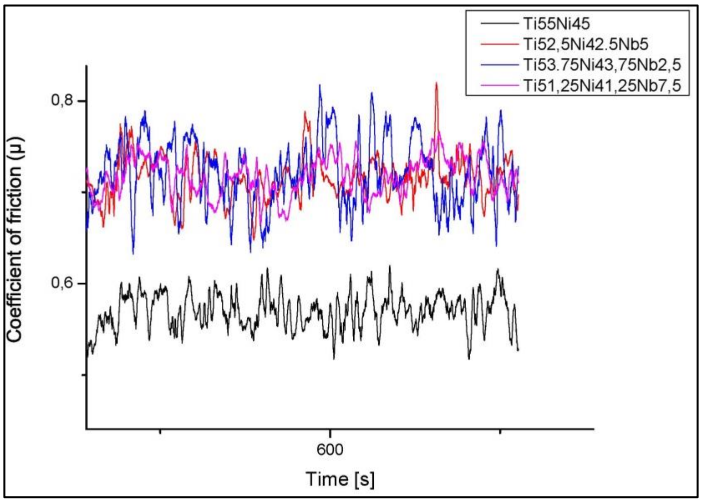

Figure 4.15: Wear results of laser deposited $Ti_{50-x/2}$ $Ni_{50-x/2}Nb_{x}$ alloy coating.

The $Ti_{55}Ni_{45}$ alloy exhibited lower coefficient of friction than $Ti_{53.75}Ni_{43.75}Nb_{2.5}$, $Ti_{52.5}Ni_{42.5}Nb_{5}$ and $Ti_{51.15}Ni_{41.15}Nb_{7.5}$. The low coefficient of friction during mechanical sliding of two component was due to the presence of less debris between the two components and the less contact area. More debris means that the material is degrading easily. Harder surfaces degrade slower than softer surface [1]. The SEM results of $Ti_{55}Ni_{45}$ in Figure 4.9(a) showed higher proportion of $NiTi_2$ phase than NiTi, and its hardness results were higher than that of TiNiNb which correlates to high wear resistance observed. High proportions of $NiTi_2$ lead to lower wear rate [1]. The addition of Nb in Ni-Ti alloy resulted in slight reduction in wear resistance as compared to $Ti_{55}Ni_{45}$. An average of 0.7 coefficient of friction was achieved above 200s which correlate to the finding by Li et al [9].

The images of worn surfaces of Ti50-x/2 Ni50-x/2Nbx alloys are shown in Figure 4-16. Series of parallel grooves longitudinal to the sliding direction were observed on all samples surfaces, the formation of grooves might be due to debris caused by abrasive wear which were trapped between the surface and the pin, thus increasing wear rate. Similar observations that create groove on the surface of the sample were reported by Neupane et al. [41]

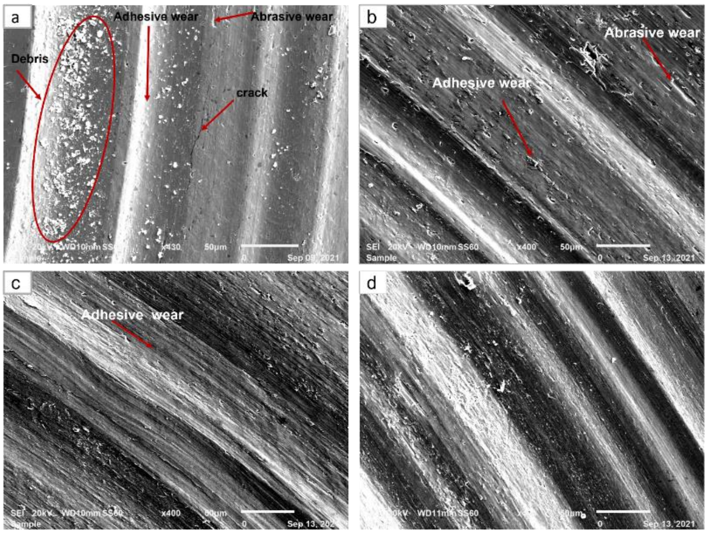

Figure 4.16 SEM images of worn $Ti_{50-x/2}Ni_{50-x/2}Nb_x$ alloys: (a) $Ti_{55}Ni_{45}$, (b) $Ti_{53.75}Ni_{43.75}Nb_{2.5}$ (c) $Ti_{52.5}Ni_{42.5}Nb_5$ and (d) $Ti_{51.15}Ni_{41.15}Nb_{7.5}$ produced at 600W and 0.5m/min

The SEM image in Figure 4.16 sample (a) shows both adhesive and abrasive wear, and debris circled in red adhered to the surface in the groove as compared to sample (b), (c) and (d). The reason for debris on sample (a) might be due to the brittleness nature of the alloy. Micro cracks were observed on sample (a) which is evidence of brittleness caused by the presence of Ti_2Ni intermetallic phase [1, 7]. Sample (b), (c) and (d) were worn in a similar manner but with more abrasive wear. From the SEM results, sample (b), (c) and (d) has an increase NiTi intermetallic phase than Ti_2Ni, the decrease in Ti_2Ni which is hard led to decrease hardness and decrease wear resistance. During wear of nitinol, thermal cycling and applied load bring about austenite-martensitic transformation, with the martensitic phase significantly increasing the wear resistance [42]. Inshort, decreasing the hardness of Ni-Ti alloy decreases the wear resistance which in turn improve machinability.

4.10. Summary of Chapter 4

This chapter presented the process development of Nb added into Ni-Ti alloy to produce a coating on Ti6AL4V. The process development included alloy development, optimisation of optimum laser cladding parameters and characterisation of NiTiNb clads produced at different laser parameter and different scanning speed. Optimum laser cladding parameters which includes good metallurgical bonding of the clad on the substrate, less dilution and good fusion were observed when laser power set a 600W and laser scanning speed set at 0.5m/min. Effect of Nb on mechanical properties and microstructure were observed, hardness and wear resistance decrease with increase in Nb. Refined dendritic structure was observed with increase in Nb. The Ti_2Ni intermetallic phase decrease with Nb addition, while TiNi increased with addition of Nb. There were crack visible on a binary Ti-Ni alloy clads, however, no crack observed on a ternary (Ni-Ti-Nb) alloy clads. The temperature hysteresis increased slightly with niobium addition

Chapter 5 Conclusions

This chapter present conclusions of the finding base on the results which include optical microscopic, SEM-EDS, DSC, XRD, hardness and wear results of laser clad produced by laser deposition of mechanically mixed powder of pure titanium, pure nickel, and pure niobium.

5.1. Summary of the findings

The aim of this work was to investigate the effects of adding niobium (Nb) on microstructural and mechanical properties of laser coated nitinol (NiTi) used for surface modification of Ti6Al4V alloy. A crack-free well bonded coating of about 1.22 mm with enhanced wear resistance was achieved with laser process parameters set at 600W laser power and 0.5m/min laser scanning speed and powder deposition rate of 2 rpm.

- Addition of niobium in a Ni-Ti binary system to form a Ni-Ti-Nb ternary alloy resulted in formation of finer dendritic microstructure.
- The addition of niobium promoted the formation of NiTi over $NiTi_2$ intermetallics.
- XRD results identified the B2(austenite), B19(martensitic), R-phase (rhombohedral) and niobium rich phases. NiTi (B2 and B19) intensity peaks increase with addition on Nb
- Temperature hysteresis slightly increased with addition on Nb
- Hardness decreased by 37% as niobium addition increased to 7.5wt.%Nb, this means, machinability was improved
- $Ti_{55}Ni_{45}$ reported slightly less coefficient of friction than to $Ti_{51.25}Ni_{41.25}Nb_{7.5}$ alloy as a results of niobium addition. Which means, addition of Nb in Ni-Ti alloy enhanced the wear resistance of Ni-Ti alloy

5.2. Recommendations

The following recommendation were made based on the results

- Employment of post heat treatment
  Post heat treatment of the coating may help reduce the hardness of the HAZ. Reducing the hardness may reduce the tendency of cracking and enhance the wear resistance.

- Investigation of tensile stress-strain behaviour of Ni-Ti-Nb alloy may also help to determine the strength of the coating.
- Machinability testing of Ni-Ti-Nb alloy may help to determine the effect of niobium on machinability

Chapter 6 References

[1] M. N. Mokgalaka, S. L. Pityana, P. A. I. Popoola and T. Mathebula, “NiTi intermetallic surface coatings by laser metal deposition for improving wear properties of Ti-6Al-4V substrates,” *Advances in Materials Science and Engineering,* 2014.

[2] J. C. Chekotu, R. Groarke, K. O’Toole and D. Brabazon, “Advances in Selective Laser Melting of Nitinol Shape Memory Alloy Part Production,” *Materials,* vol. 12.5, p. 809, 2019.

[3] S. W. Robertson, A. R. Pelton and R. O. Ritchie, “Mechanical fatigue and fracture of Nitinol,” *International Materials Reviews,* vol. 57(1), pp. 1-37, 2012.

[4] I. Polozov and A. Popovich, “Microstructure and Mechanical Properties of NiTi-Based Eutectic Shape Memory Alloy Produced via Selective Laser Melting In-Situ Alloying by Nb,” *Materials,* vol. 14(10), p. 2696, 2021.

[5] Y. Tian, C. Lin, J. Yu, Z. Liu, Y. Zhang and S. Jia, “Surface modification of TC4 Ti alloy by laser cladding with Ni-Ti-Nb powders.,” *In MATEC Web of Conferences,* vol. vol. 189, p. 01004, 2018.

[6] C. Zhang and Z. N. “. Farhat, “Sliding wear of superelastic TiNi alloy,” *Wear,* Vols. 267(1-4), pp. 394-400, 2009.

[7] F. Zhang, L. Zheng, F. Wang and H. Zhang, “Effects of Nb additions on the precipitate morphology and hardening behavior of Ni-rich Ni55Ti45 alloys,” *Journal of Alloys and Compounds,* vol. 735, pp. 2453-2461, 2018.

[8] M. E. R. Cronemberger, V. H. F. Menezes, R. D. Silva, Í. G. Santos, V. L. Sordi, S. E. Kuri and C. A. D. Rovere, “Effect of Nb Content in the Microstructural and Thermal Characteristics of NiTiNb Shape Memory Alloys,” *Materials Research,* vol. 22, 2019.

[9] Y. Li, F. Zhang, T. T. Zhao, M. Tang and Y. Liu, “Enhanced wear resistance of NiTi alloy by surface modification with Nb ion implantation,” *Rare Metals,* vol. 33(3), pp. 244-248, 2014.

[10] G. Aggarwal, S. J. Park and I. Smid, “Development of niobium powder injection molding: Part I. Feedstock and injection molding,” *International Journal of Refractory Metals and Hard Materials,* vol. 24(3), pp. 253-262, 2006.

[11] S. R. Al-Sayed Ali, A. H. A. Hussein, A. A. M. S. Nofal, S. E. I. Hasseb Elnaby, H. A. Elgazzar and H. A. Sabour, “Laser Powder Cladding of Ti-6Al-4V α/β Alloy,” *Materials 10,* vol. 10, p. 1178, 2017.

[12] C. Zhong, J. Liu, T. Zhao, T. Schopphoven, J. Fu, A. Gasser and J. Schleifenbaum, "Laser metal deposition of Ti6Al4V," *Applied Sciences,* vol. 3, p. 764, 2020.

[13] D. Gospodinov, F. Nikolay and S. Dimitrov, "Classification, properties and application of titanium and its alloys," in *Proceedings of university of ruse,* 2016.

[14] D. R. Askeland and P. P. Phule, "The science and engineering of materials," *Brooks/cole,* 2003.

[15] C. Zhong, J. Liu, T. Zhao, T. Schopphoven, J. Fu, A. Gasser and J. Schleifenbaum, "Laser metal deposition of Ti6Al4V -a brief review," *Applied Sciences,* vol. 10(3), p. 764, 2020.

[16] C. Veiga, J. P. Davim and A. J. R. Loureiro, "Properties and applications of titanium alloys: a brief review," *Rev. Adv. Mater. Sci,* vol. 32((2), pp. 133-148., 2012.

[17] K. Yang and Y. Ren, "Nickel-free austenitic stainless steels for medical applications," *Science and technology of advanced materials,* vol. 11, no. 1, 2010.

[18] J. e. Everhart, Engineering properties of nickel and nickel alloys, London: Springer Science & Business Media., 2012.

[19] R. J. Smith, G. J. Lewi and D. H. Yates, "Development and application of nickel alloys in aerospace engineering.," *Aircraft engineering and aerospace technology,* vol. 73, no. 2, pp. 138-147, 2001.

[20] S.-F. Ou, B.-Y. Peng, Y.-C. Chen and M.-H. Tsai, "Manufacturing and characterization of NiTi alloy with functional properties by selective laser melting," *Metals 8,* vol. 5, p. 324, 2018.

[21] T. E. Abioye, P. K. Farayibi, P. Kinnel and A. T. Clare, "Fuctionally graded Ni-Ti microstructure synthesised in process by direct laser metal diposition," *The International Jounal of Advance Manufacturing Technology,* vols. 79, no 5-6, pp. 843-850, 2015.

[22] J. A. Simpson, K. Melton and T. Duerig., "Nickel/titanium/niobium shape memory alloy & article," *U.S. Patent,* vol. 4, pp. 725-770, 1988.

[23] A. R. Pelton, S. M. Russell and J. DiCello, "The physical metallurgy of nitinol for medical applications," *Jom,* vols. 55(5), pp.33-37., pp. 33-37, 2003.

[24] T. Bertilsson, "Intermetallic Compound Formation in Ni-Ti-Fe Powder Mixtures," *Material Engineering,* pp. 1-2, 2018.

[25] H. C. Ling and K. Roy, “Stress-induced shape changes and shape memory in the R and martensite transformations in equiatomic NiTi.,” *Metallurgical Transactions A,* vol. 12(12), pp. 2101-2111, 1981.

[26] K. Otsuka and X. Ren, “Physical metallurgy of Ti–Ni-based shape memory alloys,” *Progress in materials science,* vol. 50(5), pp. 511-678, 2005.

[27] M. Piao, S. Miyazaki and K. Otsuka, “Characteristics of deformation and transformation in Ti44Ni47Nb9 shape memory alloy.,” *Materials Transactions,* vol. 4, pp. 337-345, 1992.

[28] G. Riva, M. Vanelli and G. Airoldi, “A new calibration method for the X-ray powder diffraction study of shape memory alloys,” *physica status solidi (a),* vol. 148(2), pp. 363-372, 1995.

[29] C. W. Chan, L. Carson and G. C. Smith, “Fibre laser treatment of martensitic NiTi alloys for load-bearing implant applications: Effects of surface chemistry on inhibiting Staphylococcus aureus biofilm formation,” *Surface and Coatings Technology,* vol. 349, pp. 488-502, 2018.

[30] M. Iijima, W. A. Brantley, W. H. Guo, W. A. T. Clark, T. Yuasa and Mizoguchi, “X-ray diffraction study of low-temperature phase transformations in nickel–titanium orthodontic wires,” *Dental Materials,* vol. 24(11), pp. 1454-1460, 2008.

[31] S. B. Alapati, W. A. Brantley, M. Iijima, S. R. Schricker, J. M. Nusstein, U. M. Li and T. A. Svec, “Micro-XRD and temperature-modulated DSC investigation of nickel–titanium rotary endodontic instruments,” *Dental Materials,* vol. 25(10), pp. 1221-9, 2009.

[32] P. Majumdar, S. B. Singh and M. Chakraborty, “Wear response of heat-treated Ti–13Zr–13Nb alloy in dry condition and simulated body fluid,” *Wear,* vols. 264(11-12), pp. 1015-1025, 2008.

[33] I. Kovaříková, B. Szewczyková, P. Blaškoviš, E. Hodúlová and Lechovič, “Study and characteristic of abrasive wear mechanisms,” *Materials Science and Technology,* vol. 1, pp. 1-8, 2009.

[34] D. A. Rigney, “Transfer, mixing and associated chemical and mechanical processes during the sliding of ductile materials,” *Wear,* vols. 245(1-2), pp. 1-9, 2000.

[35] Y. Wang and H. M. Wang, “Wear resistance of laser clad Ti2Ni3Si reinforced intermetallic composite coatings on titanium alloy,” *Applied Surface Science,* vols. 229(1-4), pp. 81-86, 2004.

[36] H. Attar, S. Ehtemam-Haghighi, D. Kent, X. Wu and M. S. Dargusch, “Comparative study of commercially pure titanium produced by laserengineered net shaping, selective laser melting and casting processes,” *Materials Science and Engineering,* vols. A,705, pp. pp.385-393, 2017.

[37] N. K. Arthur and S. Pityana, “Microstructure and materialvproperties of LeNS fabricated Ti6AL4V components,” *R&D Journal,* vol. 34, pp. 33-36, 2018.

[38] C. Hui-Chi, B. Guijun and S. Chen-Nan, “High energy beam welding processes in manufacturing,” in *Handbook of Manufacturing Engineering and Tech-nology,* 2014, pp. 617-639.

[39] M. F. Zhu, J. M. Kim and C. P. Hong, “Modeling of Globular and Dentricti StructureEvolution in Soilidification of an Al-7mass%Si Alloy,” *ISIJ International,* vol. 41, pp. 992-998, 2001.

[40] J. Li, H. Wang, J. Liu and J. Ruan, “Effects of Nb addition on microstructure and mechanical properties of TiNiNb alloys fabricated by elemental powder sintering,” *Materials Science and Engineering: A,* vol. 609, pp. 235-240, 2014.

[41] R. Neupane and Z. Farhat, “Wear mechanisms of nitinol under reciprocating sliding contact. Wear, 315(1-2), pp.25-30.,” *Wear,* vols. 315(1-2), pp. 25-30, 2014.

[42] B. Swain, S. Bajpai and A. Behera, “Microstructural evolution of NITINOL and their species formed by atmospheric plasma spraying,” *Surface Topography: Metrology and Properties,* vol. 7(1), p. 015006, 2019.

[43] B. Wysocki, P. Maj, A. Krawczyńska, K. Rożniatowski, J. Zdunek, K. J. Kurzydłowski and W. Święszkowski, “Microstructure and mechanical properties investigation of CP titanium processed by selective laser melting (SLM),” *Journal of Materials Processing Technology,* vol. 241, pp. 13-23, 2017.

[44] H. Gedda, “Laser cladding: an experimental and theoretical investigation,” Luleå tekniska universitet, 2004.

[45] S. Jiang, Y. Liang, Y. Zhang, Y. Zhao and Z. C, “Influence of addition of Nb on phase transformation, microstructure and mechanical properties of equiatomic NiTi SMA,” *Journal of Materials Engineering and Performance,* vol. 25(10), pp. 4341-51, 2016.

[46] M. Piao, S. Miyazaki, K. Otsuka and N. Nishida, “Effects of Nb addition on the microstructure of Ti–Ni alloys,” *Materials Transactions,Jim,* vol. 33(4), pp. 337-345, 1992.

[47] K. Uchida, N. Shigenaka, T. Sakuma, Y. Sutou and K. Yamauchi, “Effect of Nb content on martensitic transformation temperatures and mechanical properties of Ti-Ni-Nb

shape memory alloys for pipe joint applications," *Materials transactions,* vol. 48(3), pp. 445-450, 2007.

[48] J. Dutta Majumder and I. Manna, "Laser material processing," *International materials reviews,* vols. 5-6, pp. 341-388, 2011.

[49] J. D. Avila, S. Bose and A. Bandyopadhyay, "Additive manufacturing of titanium and titanium alloys for biomedical applications. In Titanium in Medical and Dental Applications," *Woodhead Publishing,* pp. 325-343, 2018.

[50] D. G. Bansal, O. L. Eryilmaz and P. J. Blau, "Surface engineering to improve the durability and lubricity of Ti–6Al–4V alloy," *Wear,* vols. 271(9-10), pp. 2006-2015, 2011.

[51] J. B. Fogagnolo, A. V. Rodrigues, M. S. F. D. Lima, V. Amigo and R. Caram, "A novel proposal to manipulate the properties of titanium parts by laser surface alloying," *Scripta Materialia,* vol. 68(7), pp. 471-474, 2013.

Chapter 7 Appendix A: MRS Conference paper 20

MRS Advances © 2020 Materials Research Society
DOI: 10.1557/adv.2020.158

Effects of niobium (Nb) on mechanical properties of laser coated Nitinol (NiTi) used for surface modification of Ti6Al4V alloy

B.S Skhosane[1*], M Tlotleng[1, 2], and S.L Pityana[1, 3]

[1]Laser Enabled Manufacturing National Laser Centre CSIR, Pretoria, 0001, South Africa
[2]Department of Mechanical Engineering Science, University of Johannesburg, Auckland Park Campus, Johannesburg, 2006, South Africa
[3]Department of Chemical and Metallurgical Engineering, Tshwane University of Technology, Pretoria, 0001, South Africa

Abstract:

Laser surface treatment is widely used as an engineering technique due to its special characteristics and several advantages over other surface modification techniques. In the present study, elemental mechanically pre-alloyed powder consisting of Niobium, Titanium and Nickel was deposited onto a grade 5 Titanium alloy substrates to form a high wear resistance coating. This was such that the surface mechanical properties of the base metal can be improved. The fabricated samples were characterised using optical microscopy, scanning electron microscopy (SEM) with energy dispersive spectroscopy (EDS), Differential Scanning Calorimeter (DSC), micro hardness tester and wear machine. The deposited coatings were well bonded and consisted of various phases. Hardness was seen decrease with increase in Nb content while wear resistance increasing with increase in niobium content.

1. INTRODUCTION:

Titanium and titanium alloys are widely used in manufacturing aerospace components and chemical industries components due to their outstanding properties such as high specific strength ratio, excellent corrosion resistance and good creep resistance [1, 2]. However, their use in mechanically wear conditions is limited due to their poor wear resistance properties [1, 3]. These limitations can be overcome by surface modification using surface engineering techniques. Methods such as laser cladding, nitriding and thermal spraying are amongst others constitute surface coating techniques in engineering field. Laser cladding technique is a superior surface modification technique owing to its special characteristics such as achieving good metallurgical bonding between the surface coating and the parent material with minimum dilution when compared to techniques such as thermal plasma spraying and submerge arc cladding [2]. Laser cladding uses low heat input, resulting in less distortion and minimum heat affected zone [2, 4]. This technique is often use in the refurbishment of worn parts, protection of new parent material against corrosion and hard facing of material [5].

In this study, Nitinol was laser cladded onto titanium substrate. Nitinol (Nickel-titanium or NiTi) has remarkable properties such as super-elasticity, shape memory effect (SME), good corrosion resistance and low stiffness [2, 4, 6]. A binary phase diagram shown in figure 1 indicates that Ni-Ti alloys are produced with NiTi, $NiTi_2$ and Ni_3Ti intermetallic compounds [7]. Near stoichiometric composition TiNi intermetallic forms and is responsible for the SME characteristic. Nitinol comprises of austenite phase at high temperature and martensitic structure at low temperature. For the SME, NiTi transformation is between cubic crystal structures or austenite phase denoted as B2 phase and monoclinic, martensitic called B19. The martensitic phase can occur in one or two transformation steps, either by $B2 \rightarrow B19'$ or $B2 \rightarrow R \rightarrow B19$ [7].

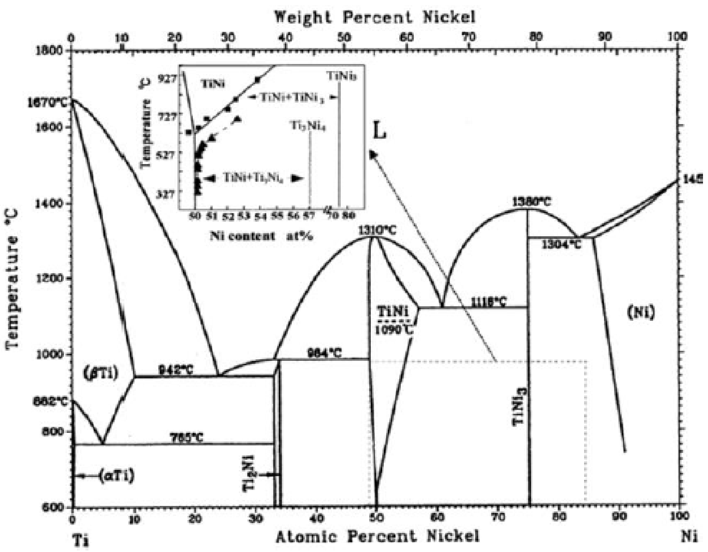

Figure 1: Binary NI-Ti phase diagram [7]

SME can either be used as a coating or to build Nitinol component [8]. Shape memory characteristics and transformation can be improved by adding niobium (Nb) to form a ternary alloy, Ti-Ni-Nb alloys that exhibits a wide transformation temperature [9]. Beritilsson [7] reported the intermetallic compound transition temperature of NiTi, it has a first endothermic peak occur in the temperature range 770 - 850°C and the second exothermic peak which occur in the temperature range 946 -953°C. Since SME alloy are widely used, Tian et al. [5] confirmed that surface modification of Ti6Al4V by laser cladding with Ni-Ti-Nb improves surface mechanical properties such as wear and hardness resistance. Hardness of the modified surface was twice that of unmodified Ti6Al4 and wear-resistance was significantly improved.

Nomsa et al [2, 4] reported surface modification of Ti6Al4V by surface laser cladding Nitinol material. Surface hardness and wear resistance were observed to have increased with an increased in Ti from Ti_{45}-Ni_{55} to Ti_{55}-Ni_{45}. Titanium in the matrix was responsible for the increase in hardness while nickel is responsible for wear resistance.

Simpson et al [6, 10] investigated the effect of niobium (Nb) addition on the shape memory effects (SME) characteristics of Ti-Ni. Martensitic start (Ms) transformation temperature was studied by differential scanning calorimeter (DSC), M_s Temperature decreases with increase in Nb.

Alloying is one of metal strengthening technique, a degree of strengthening depend on two factors: firstly, a larger difference in atomic size between the original atom and the added atom increases the strengthening effect, this is due to disruption caused on the crystal structure, and secondly the amount of the alloying [11], high amount of alloying increases the strengthening effect.

In this study, elemental mechanically pre-alloyed powder consisting of niobium, titanium and nickel was deposited onto Ti6Al4V substrates to modify its surface hardness and wear resistance. The fabricated samples were characterised using optical microscopy (OM), scanning electron microscopy (SEM) with energy dispersive spectroscopy (EDS), micro-hardness tester, and wear test machine while phase transformation temperature of the SME were measured by differential scanning calorimeter (DSC).

2. METHODOLOGY:

2.1 Materials

A mixture of elemental nickel, titanium and niobium powder with the particle size fraction ranging from +45µm to -95µm was used to produce 1 mm thick coating layer on a Ti6Al4V surface. Prior mixing, powders were weighed to achieve a nominal composition as presented in Table 1. Mixed powders were then enclosed in small plastic containers, which were then shock using a tubular powder blender. Blending was performed for twelve hours at 300 rpm so that homogeneous mixture would be produced. The advantages of using this technique is that particles size remains the same.

Table 1: Showing laser processing parameters for Ni-Ti-Nb coating on a TiC4 base plate

Powder mixture	Laser Power(W)	Laser scanning speed(m/min)	Powder feed rate(rev/min)
$Ti_{55}Ni_{45}$	600	0.5	2
$Ti_{53.75}Ni_{43.75}Nb_{2.5}$	600	0.5	2
$Ti_{52.5}Ni_{42.5}Nb_{5}$	600	0.5	2
$Ti_{51.25}Ni_{41.25}Nb_{7.5}$	600	0.5	2

2.2 Laser coating process

An IPG fibre laser with 1073 nm wavelength, 150 mm collimator, 200 µm fibre core and 300 mm lens was used for melting a stream of powder particle to create a good metallurgical bonded coating on Ti6Al4V surface. The laser cladding techniques was realized by defocusing a laser beam from an in-focus keyhole mode to give a 2 mm laser beam diameter. Powder efficiency was achieved when laser beam aligned to the powder stream injected from a 3-way nozzle mounted on a KUKA robot. The laser processing was done at 12 mm stand-off distance over a commercially α+β Ti6Al4V titanium alloy plate surface with the dimensions 50 x 50 x 5 mm while injecting stream of mixed powder particles producing a coating bead of 2 mm width and 1 mm thick. Multiple clad tracks with 50% overlap were produced to make a square build of 30*30mm with two layers.

Prior laser cladding, the plate were first sandblasted to remove possible oxides, then cleaned with acetone to remove contaminations such as oil or stains caused by cutting fluids which might introduce porosity or cracking during solidification . The deposition was scanned in two directional using a KUKA robotic arm positioning system, an argon shielding gas was blown at 12 l/min over the weld pool to prevent oxidation of the molten pool. Figure 2, shows the schematic 3way nozzle used for cladding process. Laser beam scanning speed, laser power, shielding gas rate and laser beam diameter were kept constant while varying powder composition as presented in Table 1 above.

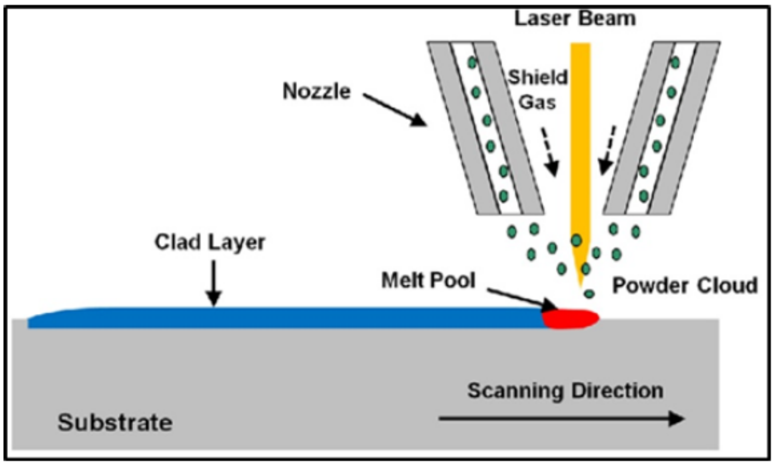

Figure 2: Schematic set-up of 3-way laser cladding process [1]

2.3 Material characterisation

Metallographic samples were sectioned across the scanning direction using the cutting machine. The sectioned pieces were hot mounted in black thermosetting Bakelite resin and thereafter ground with SiC grinding paper using water as cooling medium. There grinding was done by following the grinding sequence roughness of the grinding grit paper which was from 240, 320, 600, 800 to 1200 grit size. After grinding, the samples were polished to a mirror like finished surface of 0.04 µm using the Med-Chem polishing cloth size ranging from 9µm, 6µm, 3µm and 0.04µm using diamond suspension liquid, the polishing was done with a Struers TegraForce-5 auto/manual polisher. Thereafter sample were etched in Kroll's reagent by immersing the samples for approximately 10 seconds. The microstructures were characterised on OlympusBX51M Optical Microscope (OM) and Jeol JSM 6510 Scanning Electron Microscope (SEM) with energy dispersive spectroscopy (EDS).

3. RESULTS AND DISCUSSION:

3.1 Microstructural characterisation

Figure 3 present optical micrographs of $Ti_{50-x/2}$ $Ni_{50-x/2}Nb_x$ alloy in the order of increasing niobium.

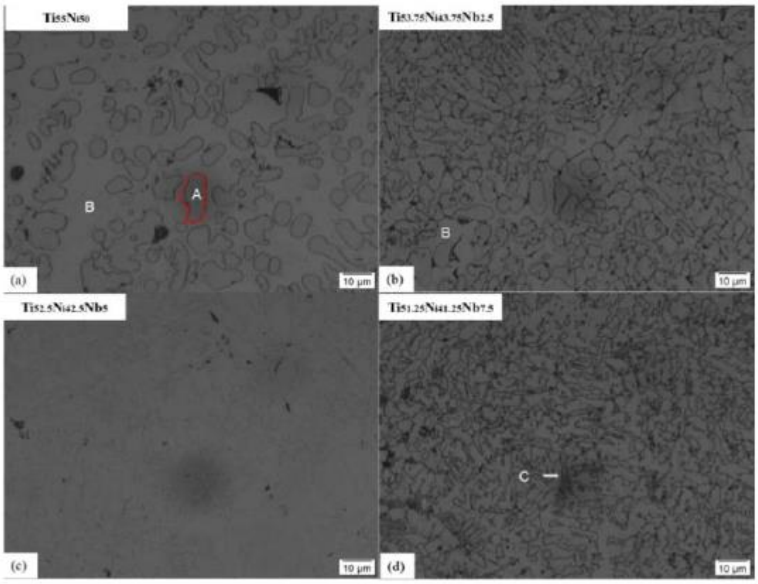

Figure 3: Optical micrographs of four typical $Ti_{50-x/2}$ $Ni_{50-x/2}Nb_x$ alloys in order of Nb addition

Structures comprises of two distinct phases as shown in figure 3 (a). A dark globular phase circled in red and labelled "A" which precipitated on a light-grey matrix labelled "B". Figure 3 (b), (c) and (d) shows dendritic phase labelled "C" in figure 3 (d) and matrix labelled "B" in figure 3 (b).

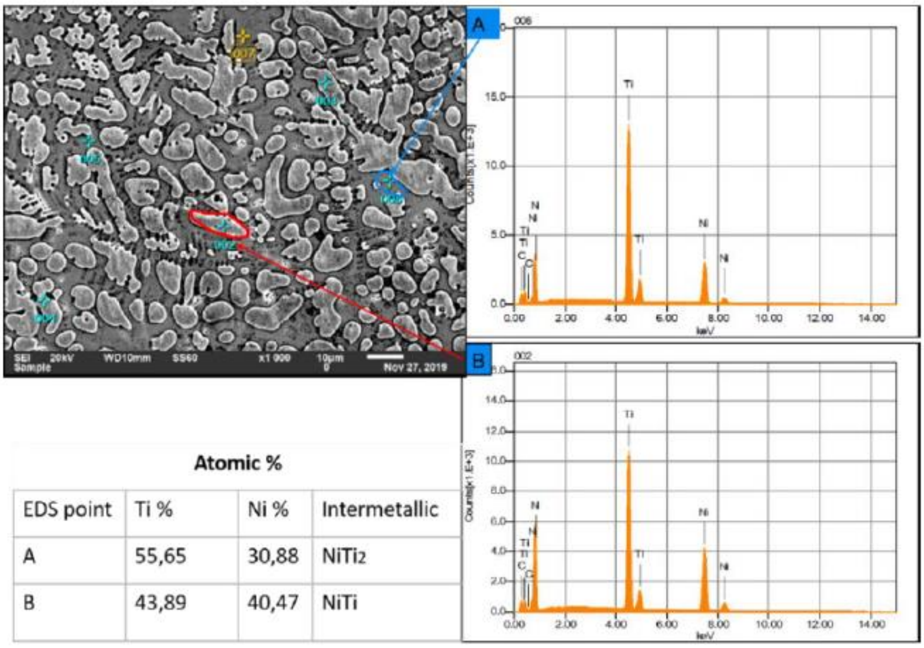

Atomic %

EDS point	Ti %	Ni %	Intermetallic
A	55,65	30,88	$NiTi_2$
B	43,89	40,47	NiTi

Figure 4: EDS analysis of $Ti_{55}Ni_{45}$

A globular light phase circled in red, in Figure 4, contained approximately equal atomic percent of Ti and Ni; this phase was therefore correlated with NiTi intermetallic. The dark-greyish matrix, circled in blue, contained approximately 1:2 atomic ratio of Ni:Ti; this was correlate to $NiTi_2$ intermetallic composition. The proportion of $NiTi_2$ is larger than NiTi, which is not good for wear resistance since $NiTi_2$ is a brittle intermetallic than NiTi. In order to increase ductile NiTi must be promoted and increase [2].

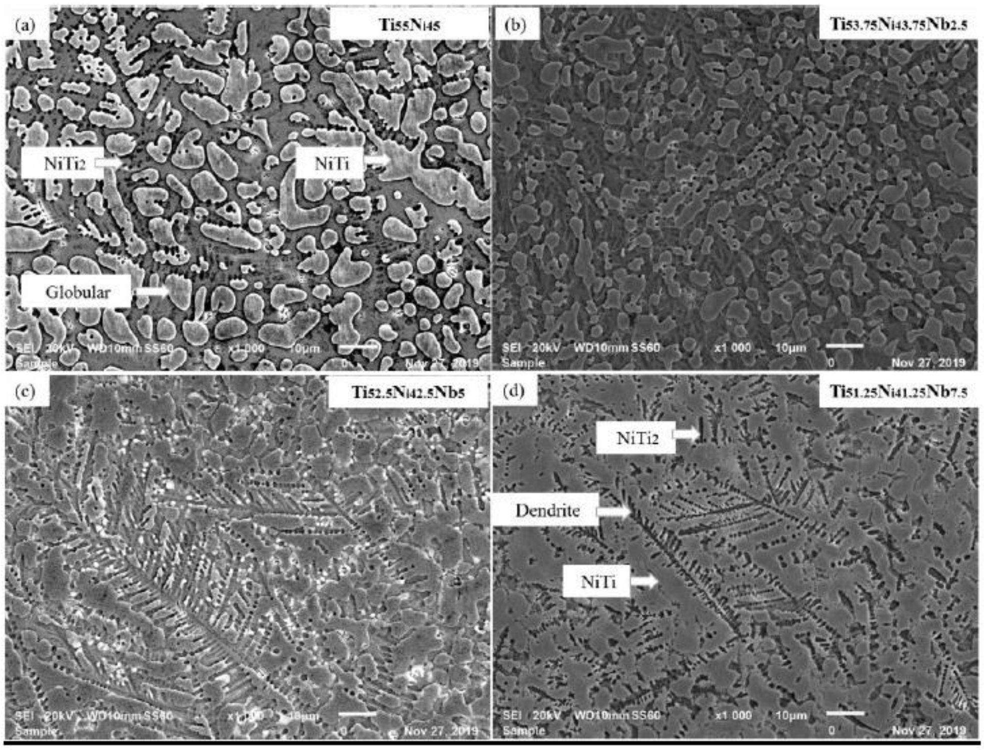

Figure 5: SEM micrographs of four typical $Ti_{50\text{-}x/2}$ $Ni_{50\text{-}x/2}Nb_x$ alloys

Figures 5(a) and (b) show light grey globular phase that was confirmed to be NiTi and a dark-grey matrix that was confirmed to be NiTi2; based on the EDS composition analysis. Effect of Nb addition was clearly realized on figures 5(c) and (d) when measuring within the dendrite and matrix. As Nb addition increases, "NiTi2" phase that is responsible for hardness decreases. NiTi, which is responsible for ductility and wear resistance, increased with addition of Nb. Globular structure (NiTi) realized on a binary alloy as shown in figure 5(a), seemed to grown bigger while the matrix transformed to finer dendrites. In short, proportion of NiTi intermetallic became extremely more than $NiTi_2$ intermetallic which is good for ductility and wear resistance.

3.2 Hardness analyses

Figure 6 present hardness measurement of the clad taken across from the top of the clad through heat affected zone and unaffected parent material area by Vickers micro-hardness tester. Indentation were loaded at 500g load, 548μm indentation spacing and dwelling time of 10sec.

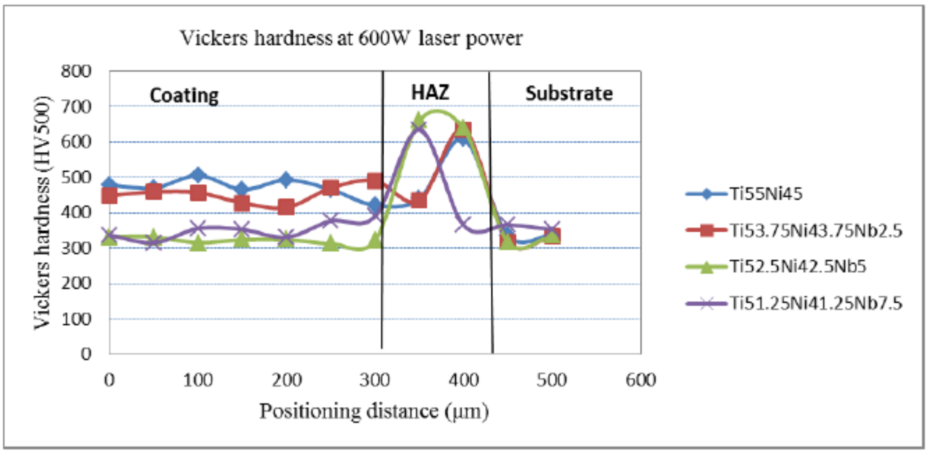

Figure 6: Microhardness profile of laser deposited $Ti_{50-x/2}$ $Ni_{50-x/2}Nb_x$ alloy coating

Micro-Vickers hardness of a binary alloy $Ti_{55}Ni_{45}$ indicate higher hardness of a coating than a parent material (Ti6Al4V) as to sample alloyed with Nb. Addition of niobium content in $Ti_{55}Ni_{45}$ resulted in decreasing the hardness of the coating. This is because Nb have complete solubility in Ti-Nb system than in Ni-Nb, which will produce more NiTi than $NiTi_2$, while $NiTi_2$ has higher hardness than NiTi intermetallic.

All sample showed higher hardness at the heat-affected zone than the coating, higher hardness correlate to martensitic structure. During laser processing, the area near the interface experience hardening heat treatment, which transform the structure to brittle martensitic structure.

3.3 Wear test results

Figure 7, present coefficient of friction versus time results measured using Tribometer version 7.3.13 which uses Ball on pin technique. A 5N (Newton) load of a steady 6mm ball pin was applied to a surface of a sample rotating at 12.9rev/s (revolution per second). sample were under friction load for a period of 25minutes. Test was done at 20°C temperature without lubrication. Prior testing, the pin was inspected for cleanliness to avoid false measurement.

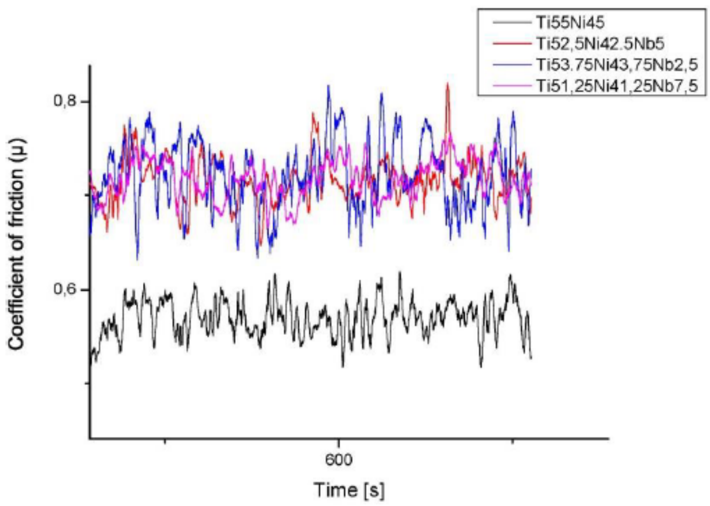

Figure 7: Wear results of $TI_{55}Ni_{45}$ and Ternary alloy Ti-Ni-Nb

Wear results for $Ti_{55}Ni_{45}$ alloy exhibits lower coefficient of friction t samples with Nb (Ti-Ni-Nb). This low coefficient friction is due to degradin surface. Harder surface degrade faster than softer surface therefore addition of resulted in softening Binary $Ti_{55}Ni_{45}$ which improved wear resistance

3.4 Differential Scanning Calorimeter

Differential scanning calorimeter results were measured using ETZSC STA 449 F3 Jupiter®. The DSC heating curve for $TI_{55}Ni_{45}$ alloy is presented in fig 8. The heating curve exhibits endothermic peak occurred at 983.3°C, at temperature, DSC curve attributes to the reaction $NiTi + NiTi3 \rightarrow NiTi$, wh occurs at 984°C [7]. On the same figure 8, the cooling curve shows eutect reaction producing exothermic peak at 977.8°C, $NiTi \rightarrow NiTi + NiTi3$

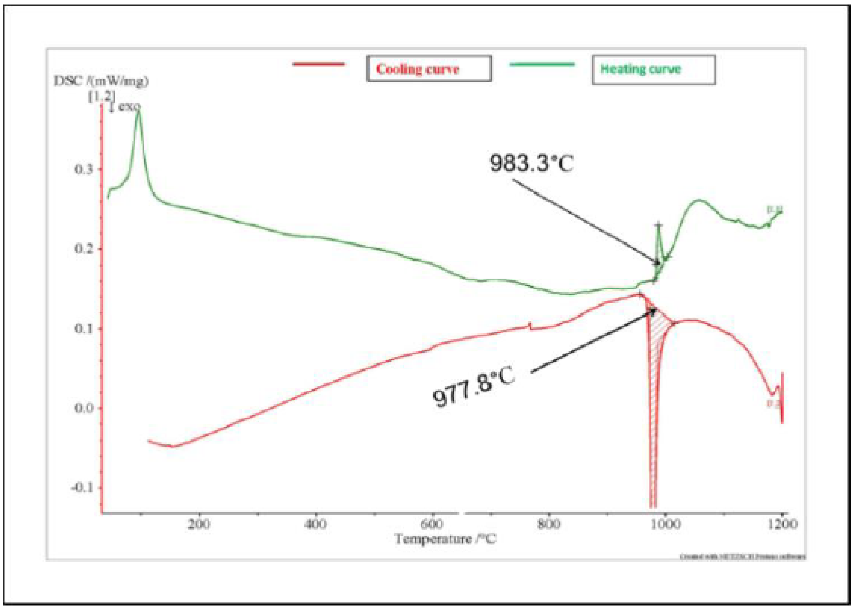

Figure 8 : DSC curve, cooling presented by red curve and heating presented by green curve

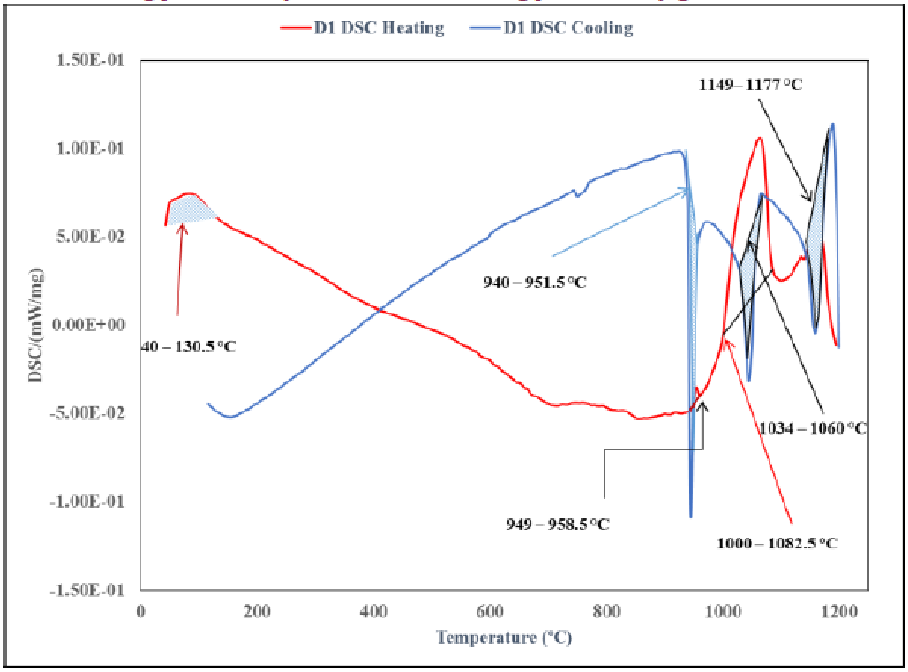

DSC heating curve for $TI_{51.25}Ni_{41.25}Nb_{7.5}$ alloy shows two feature of interest, the first is small tiny endothermic peak at 949°C – 958.5°C and the second is broad endothermic peak occurs 1000°C – 1082.5°C. The first peak attributes to allotropic transformation α-Ti to β-Ti and the second peak attributes to the reaction between NiTi + NiTi3 → NiTi which normally occurs at 984°C according Ni-Ti system.

DSC cooling curve exhibits three features, first peak occurred below 1149°C- 1177°C, second peak occurred at 1034°C -1060 °C and the 3rd feature occurred at 940°C - 951°C.5, the fist peak attributes to eutectic reaction L → NiTi + NiTi3 , second attributes to eutectoid reaction where NiTi → NiTi + NiTi3 and the third peak is allotropic transformation β-Ti to α-Ti [7]. The effect of Nb is realized on transformation temperatures, transformation temperature of $TI_{51.25}Ni_{41.25}Nb_{7.5}$ are slightly lower than transformation temperature for TI55Ni45. Again, multiple peaks were observed in $TI_{51.25}Ni_{41.25}Nb_{7.5}$ than in $TI_{55}Ni_{45}$. This confirms the study by Bertilisson [7] that alloying element promotes martensitic formation form $B1 \rightarrow R \rightarrow B19'$.

4. DISCUSSION AND REMARKS:

This work studied the effects of niobium on Nitinol during laser cladding on titanium alloy grade 5 substrates. The following can be concluded:

- Addition of niobium in a Ni-Ti-Nb ternary alloy resulted in decreasing the formation of hard intermetallic phase ($NiTi_2$). As confirmed by SEM phase analysis
- Dendritic structure was realized when niobium addition ranged between 5% - 7.5% weight percent
- Hardness decreases as niobium addition increases. This is because Nb has high solubility in Ti, which then reduces the formation of $NiTi_2$ while promoting ductile NiTi.
- Wear resistance increase as addition of Nb increases, NiTi is more ductile than $NiTi_2$
- Transformation temperature slightly increase as a results of niobium addition which is seen on DSC results

ACKNOWLEDGMENTS:

The authors would like to thank Council for Scientific and Industrial Research (CSIR) for financial support. We hope this work is going to be beneficial to industries.

REFERENCES:

[1] S. Ali, A. Hussein, A. Nofal, S. Elnaby, H. Elgazzar and H. Sabour, "Laser Powder Cladding of Ti-6Al-4V α/β Alloy," *Materials 10,* vol. 10, 2017.

[2] M. Mokgalaka, S. Pityana, P. Popoola and T. Mathebula, "NiTi intermetallic surface coatings by laser metal deposition for improving wear properties of Ti-6Al-4V substrates," *Advances in materials Science and engineering,* 2014.

[3] S.-F. Ou, B.-Y. Peng, Y.-C. Chen and M.-H. Tsai, "Manufacturing and characterization of NiTi alloy with functional properties by selective laser melting," *Metals 8,* vol. 5, p. 324, 2018.

[4] T.E.Abioye, P. Farayibi, P.Kinnel and A.T.Clare, "Fuctionally graded Ni-Ti microstructure synthesised in process by direct laser metal diposition," *Springer,* 2015.

[5] Y. Tian, C. Lin, J. Yu, Z. Liu, Y. Zhang and S. Jia, "Surface modification of TC4 Ti alloy by laser cladding with Ni-Ti-Nb powders.," *In MATEC Web of Conferences,* vol. Vol. 189, p. 01004, 2018.

[6] J. A. Simpson, K. Melton and T. Duerig., "Nickel/titanium/niobium shape memory alloy & article," *U.S. Patent ,* Vols. 4,770,725, 1988.

[7] T. Bertilsson, "Intermetallic Compound Formation in Ni-Ti-Fe Powder Mixtures," *material engineering,* pp. 1-2, 2018.

[8] J. Chekotu, R. Groarke, K. O'Toole and D. Brabazon, "Advances in Selective Laser Melting of Nitinol Shape Memory Alloy Part Production," *Materials,* vol. 12.5, p. 809, 2019.

[9] M. Piao, S. Miyazaki and K. Otsuka, "Characteristics of deformation and transformation in Ti44Ni47Nb9 shape memory alloy." *Materials Transactions,* pp. 346-353, 1992.

[10] M. Piao, S. Miyazaki, K. Otsuka and N. Nishida., "Effects of Nb addition on the microstructure of Ti–Ni alloys," *Materials Transactions,JIM 33,* vol. 4, pp. 337-345, 1992.

[11] D. R. Askeland and P. P. Phule, "The science and engineering of materials," *Brooks/cole,* 2003.